THESIS FOR THE DEGREE OF DOCTOR OF PHILOSOPHY IN
NATURAL SCIENCE, WITH SPECIALIZATION IN CHEMISTRY

MOLECULAR-LEVEL INVESTIGATIONS OF WATER-ORGANIC SYSTEMS OF ATMOSPHERIC RELEVANCE

Sofia Johansson

UNIVERSITY OF GOTHENBURG
Department of Chemistry and Molecular Biology

Gothenburg 2020

Molecular-Level Investigations of Water-Organic Systems of Atmospheric Relevance

Cover illustration: Schematic diagram of aerosol processes, Sofia Johansson.

ISBN: 978-91-7833-768-2 (print)
ISBN: 978-91-7833-769-9 (pdf)
http://hdl.handle.net/2077/62520

Department of Chemistry and Molecular Biology
University of Gothenburg
SE-412 96 Sweden

Printed by BrandFactory AB
Gothenburg, Sweden 2020

ABSTRACT

It is known that aerosol particles may have warming and/or cooling effects on the climate and negative health effects that depend on their chemical and physical properties. However, current understanding of atmospheric particles' effects is poor due to the diversity of their constituents and associated variations in properties. Important components are volatile organic compounds that are emitted from both natural and anthropogenic sources into the atmosphere and may condense onto existing particles or nucleate and contribute to formation of new particles. Organics may account for 20 to 90% of the total particle mass, and some may be enriched at particles' surfaces while others are mixed in their bulk. This may substantially influence the hygroscopicity of particles, which is highly significant as the water contents strongly affect their other physical and chemical properties. The water content may influence particle viscosity, which has feedbacks on gas-particle partitioning patterns and diffusion within the particles, and hence the chemical composition of both the gas and particle phases. The hygroscopicity also influences the critical supersaturation required for droplet activation, and thus affects cloud physics. The hygroscopicity also influences the radiative forcing of particles. However, there are needs for better fundamental understanding of interface processes on aerosol particle surfaces. Hence, ways to improve knowledge of these interactions are required. The Environmental Molecular Beam (EMB) technique can provide valuable information about the dynamics and kinetics of gas-surface interactions at near-ambient pressures. Thus, it may help efforts to elucidate processes at atmospherically relevant surfaces, and the doctoral project that led to this thesis focused on its uses, limitations and possible refinements.

The thesis is based on five papers. The first presents and evaluates improvements to an EMB instrument, involving introduction of a grated interface between high-pressure and high-vacuum regions. The improved instrument has demonstrated utility for studying water interactions with volatile surfaces at higher pressures (up to 1 Pa) than previously achievable. The grated interface also enables angular-resolved measurements, which are essential for complete understanding of the gas-

surface processes taking place during EMB experiments. The other papers present results from four EMB studies of interactions between water and organic surfaces consisting of condensed layers of nopinone, *n*-butanol and valeric acid (chosen as proxies for atmospherically relevant compounds). The investigations showed that these experimental surfaces may have water trapping probabilities close to unity, and accommodate water to varying extents. They also showed that desorption kinetics are significantly influenced by functional groups present on the surfaces, the degree to which these groups facilitate water binding, and the surfaces' phase state. Accommodation coefficients were found to range from 5 to 40% on solid surfaces and up to to 80% on liquid surfaces.

Keywords: EMB method, desorption kinetics, water uptake, organic surfaces

SAMMANFATTNING

Vi känner idag till att aerosolpartiklar påverkar både klimatet och människors hälsa på olika sätt. Den potentiellt värmande och/eller kylande effekten partiklar kan ha på klimatet, samt deras negativa hälsoeffekter beror på partiklarnas kemiska och fysikaliska egenskaper. På grund av den stora variationen av olika kemiska komponenter som bidrar till partiklar i atmosfären saknas en fullständig förståelse för partiklars påverkan på klimat och människors hälsa. Flyktiga organiska föreningar emitteras till atmosfären från både naturliga och antropogena källor, där kan de kondensera på befintliga partiklar eller bidra till bildandet av nya partiklar. Den organiska delen kan variera från 20 till 90% av den totala partikelmassan. Vissa organiska ämnen kan koncentreras i ytskiktet av partiklar och andra kan sprida sig inom partikeln och detta kan sedermera påverka partikelns förmåga att ta upp och binda vatten. Vatteninnehållet i en partikel kan påverka olika egenskaper hos partikeln på ett sätt som kan förändra partikelns viskositet och därmed begränsa och/eller möjliggöra transport mellan gas och partikelfasen samt diffusion av kemiska ämnen inuti partikeln. Detta påverkar såväl den kemiska sammansättningen av gasfasen kring partiklarna som kemin i partikeln. Hygroskopiska egenskaper hos partiklar påverkar också det övermättade ångtryck som krävs för aktivering av vattendroppar eller för att skapa iskristaller och detta har således återkopplingar på molnfysik. Vi saknar dock en grundläggande förståelsen för processer mellan gaser och olika ytor relevanta för atmosfären och vi måste hitta sätt att förbättra kunskapen på detta område. Environmental Molecular Beam (EMB) metoden som används i detta doktorandprojekt, är ett kraftfullt verktyg för att ta fram information om dynamiska och kinetiska komponenter i växelverkansprocesser mellan gaser och ytor och kan således hjälpa till att förstå liknande processer i atmosfären.

Denna avhandling bygger på fem vetenskapliga artiklar. Den första artikeln presenterar och utvärderar förbättringar gjorda på EMB-metoden, som består av ett galler mellan regionerna med högt tryck och högt vakuum i instrumentet. Den förbättrade EMB-metoden har visat sig vara en användbar teknik för studier av vattens växelverkan med flyktiga ytor

och har möjliggjort en expanderat experimentellt tryckregim upp till 1 Pa. Gallret möjliggör även vinkelupplösta mätningar, vilket är ett krav för en fullständig förståelse av växelverkansprocesser mellan gaser och ytor. Den andra till femte artikeln presenterar resultat från fyra individuella EMB-studier av vattens växelverkan med olika organiska ytor. Nopinon, *n*-butanol och valersyra har valts som representanter för organiska föreningar med koppling till atmosfären och har använts som kondensat i EMB experimenten. Studierna visar på att de organiska ytorna har en vattenupptagsförmåga på ≥ 94%. De experimentella ytorna binder vatten i olika utsträckning och desorptionskinetiken skiljer sig avsevärt beroende på de funktionella grupperna som finns tillgängliga på ytan för vatten att binda in till, samt vilken fas ytan är uppbyggd av. Upptagskoefficienten sträcker sig från 5 till 40% på fasta ytor och ökar upp till 80% på flytande ytor. Skillnader i det organiska ytskiktets tjocklek och densitet visar sig också ha betydelse för ytans förmåga att binda vatten.

Nyckelord: EMB metoden, desorptionskinetik, vattenupptagsförmåga, organiska ytor

LIST OF PUBLICATIONS INCLUDED IN THE THESIS

This thesis is based on the following five appended papers, which are referred to in the text by the corresponding Roman numerals.

Paper I

Sofia M. Johansson, Xiangrui Kong, Panos Papagiannakopoulos, Erik S. Thomson and Jan B. C. Pettersson. A Novel Gas-Vacuum Interface for Environmental Molecular Beam Studies. *Rev. Sci. Instrum.* **2017**, 88, 035112.

Paper II

Sofia M. Johansson, Xiangrui Kong, Erik S. Thomson, Mattias Hallquist and Jan B. C. Pettersson. The Dynamics and Kinetics of Water Interactions with a Condensed Nopinone Surface. *J. Phys. Chem. A* **2017**, 121, 6614–6619.

Paper III

Sofia M. Johansson, Josip Lovrić, Xiangrui Kong, Erik S. Thomson, Panos Papagiannakopoulos, Céline Toubin and Jan B. C. Pettersson. Understanding Water Interactions with Organic Surfaces: Environmental Molecular Beam and Theoretical Studies of the Water-butanol System. *Phys. Chem. Chem. Phys.* **2019**, 21, 114–1151.

Paper IV

Sofia M. Johansson, Josip Lovrić, Xiangrui Kong, Erik S. Thomson, Mattias Hallquist and Jan B. C. Pettersson. An Experimental and Computational Study of Water Interactions with Condensed Nopinone Surfaces under Atmospherically Relevant Conditions. Submitted *to J. Phys. Chem. A*

Paper V

Sofia M. Johansson, Josip Lovrić, Xiangrui Kong, Erik S. Thomson and Jan B. C. Pettersson. Water Interactions with Condensed Carboxylic Acids: Adsorption and Desorption of Water on Valeric Acid Surfaces. To be submitted to *Phys. Chem. Chem. Phys.*

LIST OF PUBLICATIONS NOT INCLUDED IN THE THESIS

Paper VI

Xiangrui Kong, Erik S. Thomson, Panos Papagiannakopoulos, **Sofia M. Johansson** and Jan B. C. Pettersson. Water Accommodation on Ice and Organic Surfaces: Insights from Environmental Molecular Beam Experiments. *J. Phys. Chem. B* **2014**, 118, 13378–13386.

Paper VII

Xiangrui Kong, Josip Lovrić, **Sofia M. Johansson,** Nønne Prisle and Jan B. C. Pettersson. Towards a Molecular Understanding of Organic-organic Interactions: Dynamics and Kinetics of Methanol on Nopinone Surfaces. To be submitted to *J. Chem. Phys.*

CONTRIBUTIONS TO PAPERS

Paper I

Sofia M. Johansson (SJ) was the main author of this paper together with Jan B. C. Pettersson. SJ conducted all the experiments and data analysis for the method evaluation, and assisted Xiangrui Kong in the DSMC simulations.

Paper II

SJ was the main author of this paper together with Jan B. C. Pettersson. SJ conducted all the experiments and performed the data analysis.

Paper III

SJ was the main author of this paper together with Josip Lovrić who wrote the simulations section. SJ conducted all the EMB experiments and performed the data analysis.

Paper IV

SJ was the main author of this paper together with Josip Lovrić who wrote the simulations section. SJ conducted all the EMB experiments and performed the data analysis.

Paper V

SJ was the main author of this paper together with Josip Lovrić who wrote the simulations section. SJ conducted all the EMB experiments and performed the data analysis.

LIST OF ABBREVIATIONS

α	Sticking coefficient
AP-XPS	Ambient Pressure X-ray Photoelectron Spectroscopy
CCN	Cloud Condensation Nuclei
DSMC	Direct Simulations Monte Carlo
ELVOC	Extremely Low Volatility Organic Compound
EMB	Environmental Molecular Beam
ESEM	Environmental Scanning Electron Microscopy
ETEM	Environmental Tunneling Electron Microscopy
HOPG	Highly Oriented Pyrolytic Graphite
HOM	Highly Oxidized Molecule
HV	High Vacuum
IS	Inelastic Scattering
IPCC	Intergovernmental Panel on Climate Change
k	Desorption rate coefficient
LVOC	Low Volatility Organic Compound
MB	Molecular Beam
MD	Molecular Dynamics
NEXAFS	Near Edge X-ray Adsorption Fine Structure
PID	Proportional-Integral-Derivative
P_{IS}	Probability of Inelastic Scattering
P_{TD}	Probability of Trapping Desorption
QMS	Quadrupole Mass Spectrometer
SOA	Secondary Organic Aerosol
SVOC	Semi-volatile Organic Compound
TD	Thermal Desorption
TOF	Time of Flight
UHV	Ultra-high Vacuum
VOC	Volatile Organic Compound

TABLE OF CONTENTS

1. THE COMPLEX ATMOSPHERE

The Earth's atmosphere is primarily composed of air that largely consists of nitrogen (≈ 78% w/w), oxygen (≈ 21% w/w) and argon (≈ 1 % w/w).[1] However, what we breathe is much more complex, because it also includes trace gases such as CO_2 and CH_4, water vapor (≈ 1–5% w/w), organics and aerosol particles.[1] Trace gases and particles are emitted into the atmosphere from both natural and anthropogenic sources (Fig. 1, step I), and play significant chemical and physical roles relative to their small amounts. Some primary aerosol particles from natural sources include salt particles from sea spray, mineral dust from wind erosion of sand and rocks, and ash from volcanic eruptions. In addition to particles, some sources emit gas phase compounds into the atmosphere. Primary emissions can participate in reactions leading to chemical transitions and contribute to secondary particle formation. Vegetation is a major natural contributor of secondary particles, as it emits large amounts of Volatile Organic Compounds (VOCs) that can be oxidized in the atmosphere (Fig. 1, step II).[2] There are also anthropogenic sources of VOCs, as well as nitrates and sulfates, which all contribute to secondary particle formation.[2] As noted by the Intergovernmental Panel on Climate Change (IPCC) report for policy-makers from 2013, both trace gases and particles influence the climate through radiative forcing.[3] However, while climate impacts of trace gases are relatively well quantified, the forcing from particles is the most uncertain of all recognized factors.[4–5] This is because there are highly complex variations in particles' chemical and physical properties, which govern their climatic effects.

Particles may contribute to direct cooling or warming of the atmosphere by scattering or absorbing radiation.[3] However, the extent of this contribution is not exactly known, mainly due to the large variety of particle components present. Some particles may, for example, scatter sunlight thereby cooling the atmosphere, while others with different composition may absorb sunlight and thus contribute to warming of the atmosphere. Particles also influence climate indirectly, by altering properties of clouds, like their albedo and lifetime.[6–8] Numbers of particles correlate with numbers of potential Cloud Condensation Nuclei (CCN). Large numbers

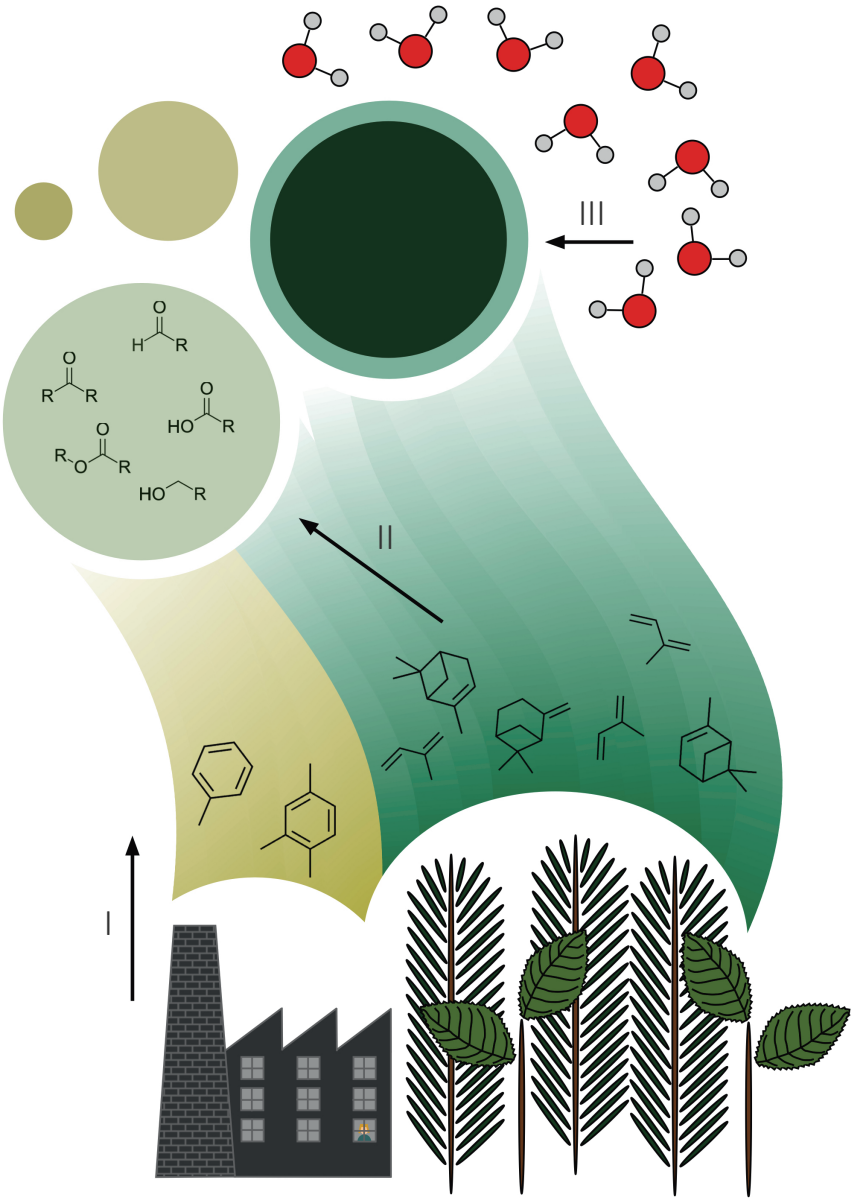

Figure 1. A schematic view of aerosol processes. I VOCs are emitted into the atmosphere where they are rapidly oxidized to form less volatile compounds. II The oxidized compounds partition to the particle phase. III Water interacts with condensed organic surfaces in the atmosphere.

of small cloud droplets results in more reflective clouds, and thus have a cooling effect on the climate.[6] Numbers of small cloud droplets are also negatively correlated with precipitation rates, and thus positively

correlated with their duration in the air, which in turn influences the global water cycle.[8] The complex cocktail of compounds present in atmospheric particles complicates absolute quantification of particles' climatic effects. Thus, in order to make good predictions of the future climate, more research is needed on the variety of aerosol components and processes influencing particle properties.

In addition to their climatic effects, aerosol particles can have strong adverse effects on human health, which depend on their composition, size and shape. Small particles penetrate deeply into our respiratory system and thus generally have stronger negative impacts on human health than coarser particles. When particles reach lung tissue they can cause inflammation, cellular changes and scarring. Moreover, both small and soluble particles may penetrate into the cardiovascular system, potentially causing diverse symptoms, such as respiratory and cardiovascular stress and disease, which frequently increase mortality rates.[9] There are also correlations between health effects and both particle dosage and exposure time: long exposure to relatively low particle concentrations may be as bad as short exposure to high particle concentrations.[9]

Water is one of the most important components in the atmosphere and it plays a crucial role in aerosol properties, partly because particles' hygroscopicity affects its other physical and chemical properties. Moreover, the hydrophilicity or hydrophobicity of their surfaces strongly influence gas to particle partitioning.[10–16] Particles' viscosities are also influenced by aerosols' water contents, and affect diffusion parameters in the particle phase, thereby influencing the chemical composition of the atmosphere.[17,18] Furthermore, particles' water as well as impurity contents influence the efficiency of cloud droplet formation, by shifting the water vapor supersaturation required for formation and droplet growth, which can strongly affect cloud micro physics.[10,12] Particles' water contents also have important feedback effects on the optical and radiative properties of interacting aerosols and clouds.[5]

Due to these important effects of water on aerosol properties, and the severity of anticipated effects of global change, there are urgent needs to improve understanding of the fundamental processes that govern

interactions between water and aerosols (Fig. 1, step III). Thus, these interactions were core concerns of the doctoral studies this thesis is based upon.

2. AIM AND MOTIVATIONS

The primary aim of the doctoral project this thesis is based upon was to improve understanding of how water interacts with various types of organic surfaces in conditions relevant for aerosol systems in the atmosphere. For this purpose, my colleagues and I (hereafter we) applied the Environmental Molecular Beam (EMB) technique, which has unparalleled capacities for detailed investigations of molecular interactions between water and organic surfaces. The project began by tackling instrumental challenges, aiming to improve the maximum experimental pressures and temperatures to increase the similarity of the experimental and tropospheric conditions. The project focused mainly on processes at interfaces of water and organic surfaces exposing various functional groups to increase fundamental understanding of organic aerosols' uptake of water, and associated interactions with it.

The specific aims of the studies described in the papers were as follows.

Paper I: to characterize and evaluate an improved EMB experimental setup, the main feature of which was a new high-vacuum/high-pressure interface.

Papers II and IV: to investigate water interactions with a biogenic Secondary Organic Aerosol (SOA) component at low temperature (Paper II) and across a broader temperature interval in combination with supporting MD simulations (Paper IV).

Paper III: to investigate water interactions with alcohols, and their influence on water uptake in relation to a phase change of the organic layer.

Paper V: to investigate water interactions with carboxylic acids.

3. A MOLECULAR-LEVEL APPROACH

Water condensation from vapors into liquid water can be explained using bulk thermodynamics, which describes the driving force as a reduction of the total free energy of the system. On macro-scale concepts such as condensation and evaporation can be used to describe water gas-surface interactions. At a molecular level, condensation and evaporation are simply molecular adsorption/absorption and desorption processes. The averaged interactions taken into account in bulk thermodynamics can be separated into individual molecular interactions where molecules are attracted and repelled by one another depending on their molecular structure and individual force fields. The molecules' ability to thermalize with a surface and form bonds governs the adsorption and desorption processes.

3.1 Water interactions with surfaces

As a water molecule impinges on a surface it may interact with molecules present on that surface through intermolecular forces, and depending on the surface composition the interactions may range from Van der Waals attraction or repulsion to ionic bonds. Hydrogen bonds, which are present in liquid or solid water, are relatively weak interactions, with energies ranging from 20 to 25 kJ mol^{-1}, and they can be formed between any electronegative atom such as nitrogen or oxygen and a less electronegative atom such as hydrogen. In pure water, molecules bind to neighboring molecules through several hydrogen bonds. However, hydrogen bonds can also be formed between water and oxidized hydrocarbons. If water molecules impinge from the gas phase onto a surface and encounter carbonyl or alcohol moieties they can interact with, they may be trapped on the surface in a weakly bound state due to Van der Waals forces such as hydrogen bonding (Fig. 2). The stronger the bonds water molecules can make with the surface, the more likely they are to remain on the surface for longer times and participate in subsequent processes.

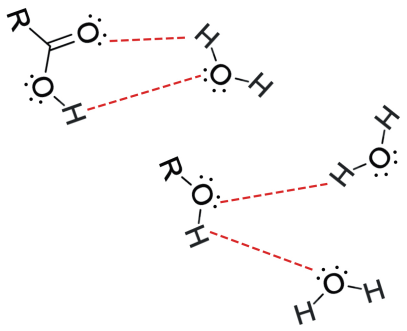

Figure 2. Hydrogen bonding between a carboxylic acid and a water molecule (top), and an alcohol and two water molecules (bottom).

3.2 Organic surfaces in the atmosphere

Organics on atmospherically relevant surfaces often originate from VOCs, which are emitted by both natural and anthropogenic sources. The organic fraction may account for 20 to 90% of particles' masses depending on the location and surrounding environment.[19] These organic compounds are molecules that are characterized by a hydrocarbon structure with or without other attached functional groups. Organics present in the atmosphere may cover a wide range of volatility and are often categorized accordingly, e.g. as Extremely Low-volatility, Low-volatility or Semi-volatile Organic Compounds (ELVOC, LVOC and SVOC respectively).[20,21] The volatility of an organic compound, which refers to its likelihood of being in the gas phase rather than a particulate phase, depends on its overall molecular structure and attached functional groups. A large fraction of the VOCs emitted by both anthropogenic and biogenic sources are unsaturated hydrocarbons such as aromatic compounds or terpenes (Fig. 3a–e).[22] Delocalized electrons in the hydrocarbon structure reduce the compounds' stability and increase their susceptibility to reaction with oxidants (primarily OH, O_3 and NO_2) in the atmosphere.[23] Such oxidation reactions initiate complex reaction mechanisms in which the primary molecule is oxidized, stepwise, into more oxygen-rich

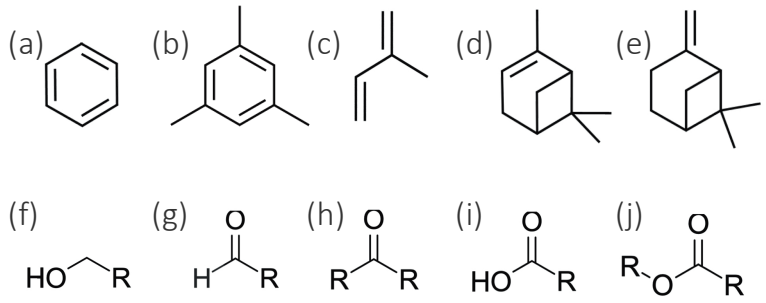

Figure 3. Chemical structures of: (a) benzene and (b) 1,3,5-trimethylbenzene (two common anthropogenic VOCs); (c) isoprene, (d) α-pinene and (e) β-pinene (three common biogenic VOCs); (f) an alcohol, (g) an aldehyde, (h) a ketone, (i) a carboxylic acid and (j) an ester (common oxidation products and primary emissions of VOCs in the atmosphere).

molecules (Highly Oxidized Molecules, HOMs).[21] The addition of oxygen atoms to the molecules usually reduces their volatility and likelihood to partition to the particle phase. The oxidation may take diverse routes through intermediary compounds and break up the molecules into various smaller components. Common compounds found along the oxidation pathways of VOCs and primary emissions including alcohols, aldehydes, ketones, carboxylic acids and esters (Fig. 3f–j).[24–26] If the saturation vapor pressure of oxidized VOC is low enough they may condense onto pre-existing particles or nucleate to form new particles.[2,21] The reacted organics can stay in the gas phase or partition to the particle phase, and they are referred to as Secondary Organic Aerosol (SOA).[27] SOA particles can contain complex mixtures of organic and inorganic components with a wide range of water contents, and they can be solid, liquid or even glassy, depending on their chemical composition and physical conditions.[18] SOA particles can be homogeneously or heterogeneously mixed, or SOA components can coat solid cores of (for example) mineral or soot particles. The composition, size and shape of aerosol particles strongly influence their chemical and physical properties.

Due to the high complexity of the different phases and compounds present in atmospheric SOA, simplifications are essential when modeling these

systems. One simplification is to group compounds based on functional groups and study their common behavior. For these reasons, compounds of three classes were chosen to form experimental surfaces in my PhD project: a ketone (terpenoid), an alcohol and a carboxylic acid. Differences in their water uptake and interactions were then explored. The selected molecules are commonly present in aerosol particles in the atmosphere, and/or have suitable chemical and physical properties (such as functional groups, vapor pressures or melting points) for the experimental settings, rendering them relevant proxies for SOA compounds in the atmosphere.

3.3 Molecule-surface interactions

Molecules impinging on a surface may either be scattered following the collision or tapped on the surface (Fig. 4). Light, inert molecules such as helium that have high incident kinetic energy may preserve their energy in the interaction with the surface and be scattered elastically. Conservation of momentum dictates that these elastic collisions result in specular scattering. However, elastic scattering events are rare and most of these interactions involve energy transfer between the impinging molecule and surface. The amount of energy transferred will depend on the properties of both the surface and impinging molecule. Molecules that transfer kinetic energy to the surface may still scatter inelastically. Such molecules may

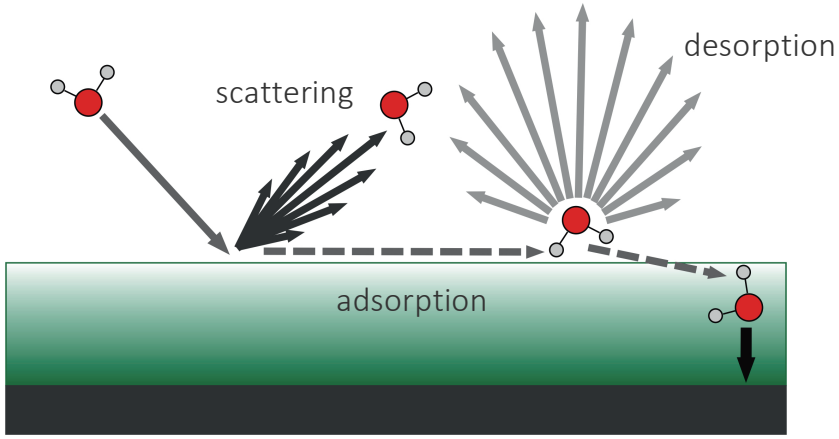

Figure 4. Schematic diagram of the scattering, adsorption and desorption processes of water impinging on an organic surface.

leave the surface in directions that depend on their incident trajectory and the local surface environment they encounter in the collision. Molecular scattering events mainly involve molecules with high kinetic energy, thus they are relatively rare in the atmosphere.

Molecules that lose most of their incident kinetic energy in collisions are trapped on the surface. These molecules thermalize with the surface, and interact with the surface with energies in van der Waals force to covalent bond ranges.[28] The trapped molecules observed in EMB experiments do not form chemical bonds and may diffuse on the surface layer in a physisorbed state. When molecules are thermalized on a surface the 'memory' of their incident speed and direction is lost. In other words, if trapped molecules can overcome the energy barrier needed to break their weak interaction with the surface they will desorb with equal likelihood in all directions (Fig. 4). For thermal desorption, this results in a typical cosine distribution as a function of the angle of desorption relative to the surface normal direction.[29,30] Molecules that bind more strongly to the surface may be accommodated there or become incorporated in the bulk, and thus change the composition and properties of the condensed phase.

The following section describes experimental methods that can be used to study the kinetics and dynamics of gas-surface interactions.

4. METHODOLOGY

Experimental techniques used in surface science have been constantly evolving in recent decades. Today, diverse methods are available for studying molecular-level gas-surface processes, which have overcome the challenge of probing high vapor pressure surfaces in the required Ultra High Vacuum (UHV) experimental conditions. Examples include microscopy and spectroscopy techniques, such as Environmental Scanning and Tunneling Electron Microscopy (ESEM and ETEM, respectively),[31–33] Near Edge X-ray Adsorption Fine Structure (NEXAFS) spectroscopy,[34] and Ambient Pressure X-ray Photoelectron Spectroscopy (AP-XPS).[35,36] In these techniques, electrons or photons are used to probe a condensed surface layer within an enclosed reaction cell. A major advantage of these techniques is that the probing particles (electrons or photons) have small cross-sections, and thus low probabilities of collision with background gases, which enables use of near-ambient experimental pressure conditions in the reaction cells. ESEM, ETEM, NEXAFS and AP-XPS may provide valuable information about the surface structure of a probed substance and composition of the bulk, such as changes in chemical composition due to a reaction between the surface molecules and a dosed vapor. However, they provide limited information about direct molecular-molecular interaction kinetics and dynamics. In contrast, molecular Beam (MB) techniques are well-established techniques for studying interactions between molecules and surfaces.[37] Recent improvements to the techniques, including use of wetted wheels and liquid jets,[38] and environmental chamber setups,[39] enable studies of molecular interactions with volatile surfaces. The EMB technique (which were used in studies underlying this thesis) can provide unparalleled information about the kinetics and dynamics of gas molecules' interactions with both solid and liquid volatile surfaces at near-ambient pressures.

4.1 The EMB method

In EMB analyses, gas pulses of water molecules are directed onto a surface substrate and the resulting time-resolved fluxes from the surface are monitored by mass spectrometry. Such experiments generate Time of

Flight (ToF) distributions of water intensity over time. In traditional MB setups, High Vacuum (HV) conditions are required to allow a sufficiently long mean free path for the beam molecules to travel and to keep the surface substrate sufficiently free from impurities. However, in EMB setups, the gas-surface interactions occur in an environment that facilitates production of condensed surfaces of volatile compounds during experiments. This enables investigations of high-vapor pressure surfaces in combination with the required HV conditions in connected chambers.

The EMB apparatus consists of a differentially pumped UHV system, separated into four chambers. The main components of the experimental setup are visualized schematically in Figure 5. A flow of helium carrier gas and D_2O is introduced into the first vacuum chamber by a pulse-generating leak valve (the MB source). D_2O is the monitored beam

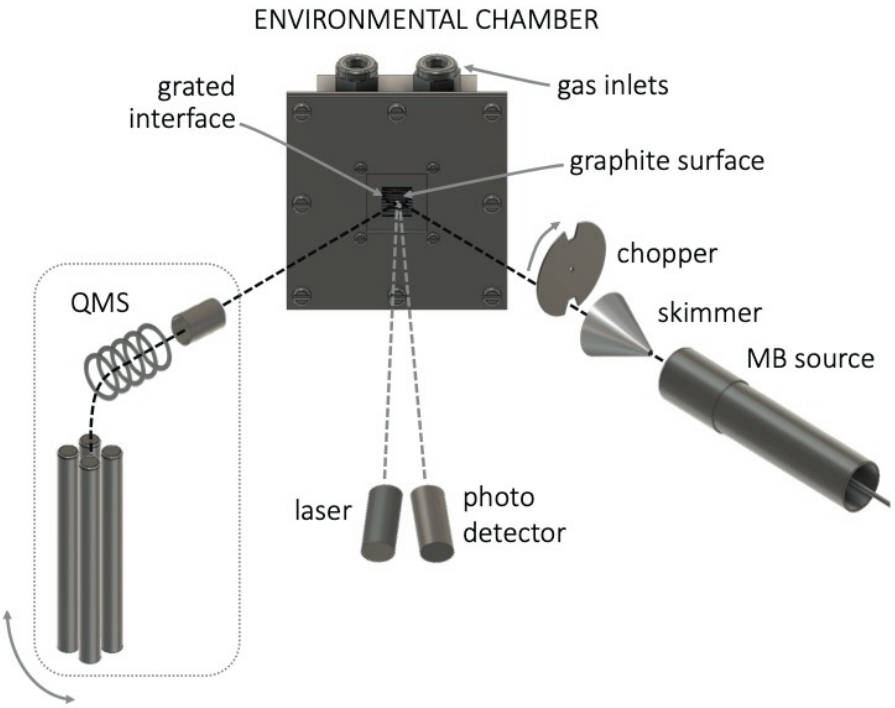

Figure 5. A schematic view of the EMB setup, showing the molecular beam (MB) source, skimmer and rotating chopper to the right and Quadrupole Mass Spectrometer (QMS) to the left. The environmental chamber is situated in the center and the molecular and laser beams are visualized as black and grey dashed lines, respectively.

molecule, selected because it can be readily differentiated from H_2O in the background gas. A skimmer and rotating chopper (rotation frequency = 120 Hz) in an adjacent vacuum chamber select beam molecules with a narrow angular spread and uniform velocity. Typically, this results in an MB with low-density pulses ($N \approx 10^{11}$ molecules) and average velocity ranging from 1400 to 1750 m s^{-1} (E_{kin} = 20–30 kJ mol^{-1}).

The MB enters the environmental chamber (Fig. 6a) through a grated interface (Fig. 6b) and impinges on a surface substrate with an incident angle of 43–45° with respect to the surface normal. The temperature of the surface substrate, a 5×5 mm^2 Highly Oriented Pyrolytic Graphite plate (HOPG) plate, is controlled by Proportional-Integral-Derivative (PID) heating and liquid nitrogen cooling. After colliding with the surface, molecules exit the environmental chamber through the same grated interface back into the UHV region. A rotatable Quadrupole Mass Spectrometer (QMS) detects the molecular flux in different directions from the surface, and can be adjusted to quantify the incident beam.

Volatile compounds of interest can be introduced into the environmental

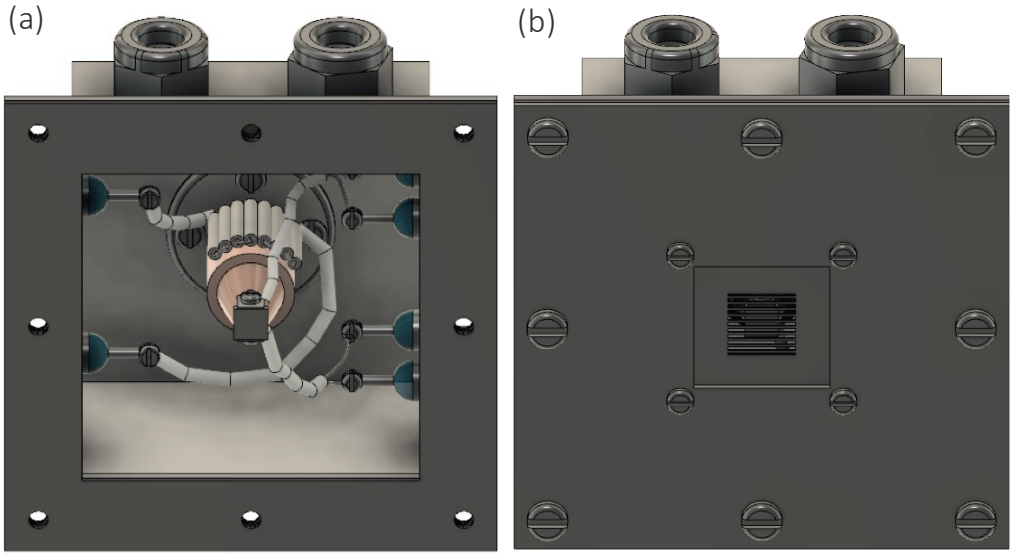

Figure 6. A schematic view of the (a) open and (b) grated environmental chamber with the graphite surface in the center situated on a copper cold finger and connected to heating filaments.

chamber during experiments to study their molecular interactions with condensed layers. The condensation and evaporation of volatile compounds are monitored with helium and light scattering. A condensed layer of micrometer thickness is usually formed in the beginning of each experiment and the layer is maintained at steady state throughout the measurements by adjusting the dosing rate. Impurities are removed from the graphite substrate between measurements by heating it to 600 K.

4.1.1 Generating experimental surfaces

In the beginning of each experiment a condensed layer of the volatile compound of interest is formed by introducing its vapor into the environmental chamber. The condensation process is monitored using helium and light (red laser, 670 nm, 860 μW) scattering.[40] Helium scatters elastically from the macroscopically smooth graphite surface substrate, and as the crystal is coated with up to a monolayer the scattering signal rapidly decreases. As the dosage is increased further a thicker layer starts to grow and is detected by light scattering. The signal from the laser changes as a multilayer grows or shrinks on the surface substrate, due to constructive and destructive interference arising from the graphite-condensate and condensate-gas interfaces. This enables monitoring of the formation process of a molecularly thin coating (with helium scattering) and thicker layer (with laser scattering) on the graphite substrate, and maintenance of the layer in a steady state during experiments by adjusting the dosage. The helium and laser signals from a graphite surface at surface temperature $T = 200$ K as *n*-butanol vapor is introduced into the environmental chamber are shown in Figure 7. The leak valve is opened at time I and almost instantly a monolayer forms on the surface and the helium signal drops, then eventually the layer grows thicker and the laser signal starts oscillating. The gas inlet is adjusted at time II to keep the condensed layer at steady state, as in experiments. The leak valve is completely closed at time III, and eventually the condensed layer evaporates, which may be observed in the oscillating laser signal, and as the monolayer evaporates the helium signal also increases.

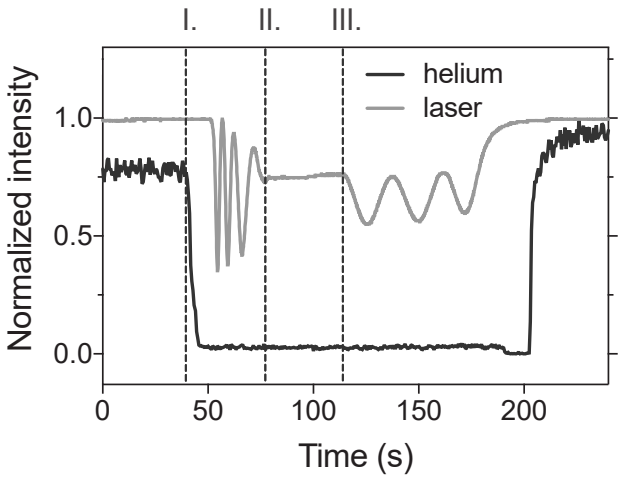

Figure 7. Normalized helium (black line) and laser (grey line) scattering during *n*-butanol condensation and evaporation on graphite.

The thickness of the layer d can be estimated from the laser signal during the condensation process:

$$d = \frac{m_d \lambda}{2\eta \cos\varphi}. \qquad \text{Eq. 1}$$

Here, m_d is the number of oscillations, λ is the wavelength of the light, η is the refractive index of the condensed molecule and φ is the angle at which the light hits the surface relative to the surface normal. In the preparation of all the experimental surfaces four oscillations are observed and $\varphi = 3°$. The refractive index and resulting layer thickness for each of the coating compounds used in the experiments are given in Table 1.

Coating compound	η	$d\ (\mu m)$
n-butanol	1.40	0.96
nopinone	1.48	0.91
valeric acid	1.41	0.95

TABLE 1. Refractive indices η and layer thicknesses of the experimental coating compounds.

4.1.2 Evolution of the EMB method

The first inner chamber (Fig. 8a, EMB 1.0) used in MB experiments was a cylindrical tube (diameter, 90 mm) with a 7 mm high and 200 mm wide slit opening.[41] A 12×12 mm^2 graphite substrate was situated in the center of the chamber, resulting in an approximately 90 mm flight path in the

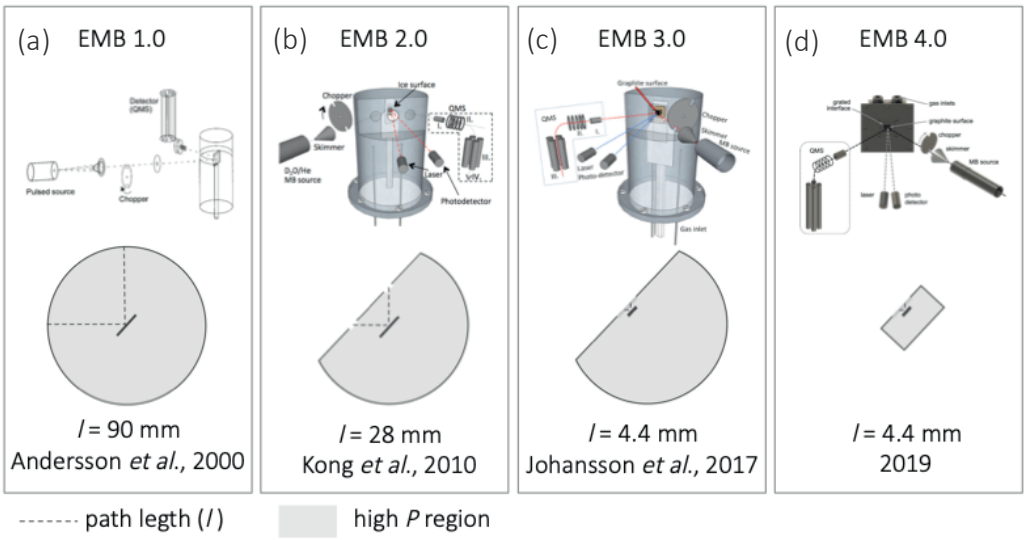

Figure 8. Schematic views of experimental EMB setup versions (a) 1.0, (b) 2.0, (c) 3.0 and (d) 4.0, with sketches of the environmental chamber (high *P* region) viewed from the top, and path lengths for molecules in the high *P* region.

high-pressure zone for molecules that scattered in the specular direction from the surface. An advantage of the wide slit opening was the possibility to acquire angular-resolved measurements, which provide good insights into the molecular level processes occurring on the surface. However, the large opening prevented attainment of high experimental pressures, and transmission of beam molecules was a limiting factor due to the long travel path. Hence, there were needs to reduce the travel distance in the high-pressure zone and improve the setup so that a higher pressure could be maintained in the inner chamber during experiments.

A new environmental chamber (Fig. 8b, EMB 2.0) was developed by removing a third of the cylindrical tube wall and replacing it with a flat

wall.[42] The new front wall had two circular openings (diameter, 0.6 mm) situated on opposite sides of the surface substrate, one for the entering beam and one for the reflected flux at the specular angle (45°) with respect to the surface normal. Apart from the two circular openings, the chamber was completely separated from the high-vacuum region. The new layout reduced the flight path in the high-pressure region to 28 mm and enabled maintenance of higher and more evenly distributed pressure over the surface during experiments. However, the new setup provided limited information on gas-surface processes as the observation angle was restricted to one direction, and the relatively long flight path led to transmission losses at high experimental pressures.

To meet the abovementioned challenges, in EMB version 2.0 the two circular openings between the high-vacuum and high-pressure zones were replaced with a new interface, a grated window (shown mounted on the current chamber in Figure 6b).[39] The area of the grated opening is 10×10 mm^2, and the bars aligned parallel to the MB are 400 μm thick, 60 μm high and spaced 140 μm apart, covering about 30% of the opening. In the new setup (Fig. 8c, EMB 3.0) a 5×5 mm^2 surface substrate was situated 1.6 mm behind the grated interface, resulting in a 4.4 mm flight path for molecules scattered at the specular angle in the high-pressure zone. The grated opening enabled angular resolved measurements at relatively high experimental pressures with little transmission losses.

However, like earlier models, EMB 3.0 had limitations in maintaining high pressures inside the environmental chamber and was thus unsuitable for studying condensed phases at high temperatures. This was mainly due to cold components in the environmental chamber connected to the surface cooling system, which acted as condensation sinks during experiments, resulting in substantial reductions of the experimental pressure in the environmental chamber. This problem was diminished by the introduction of a completely new environmental chamber in EMB 4.0 (Fig. 8d).[43] In the new layout the environmental chamber is cuboid, with a 75 cm^3 volume, and has the same grated opening and surface substrate positions as in EMB 3.0. The graphite surface is situated on a liquid nitrogen-cooled copper finger with heating filaments on top (Fig. 6a). Consequently, the cold areas

in the environmental chamber are substantially reduced, enabling higher experimental pressures.

4.1.3 Characterization and evaluation of the new high-pressure/high-vacuum interface (Paper I)

In attempts to identify the optimal interface and experimental setup for EMB 3.0, Direct Simulations Monte Carlo (DSMC) calculations were employed. The method simulates rarefied gas flows in conditions with Knudsen number (Kn) $\geqslant$ 1.[44] Such conditions prevail in non-turbulent systems where the molecular mean free path is equal to or greater than a representative physical length scale of the system. The molecules in the simulations represent an ensemble of real molecules in a probabilistic three-dimensional model, which yields detailed pressure gradients. Several layouts have been studied with variations in the high-vacuum/high-pressure interface and both the surface shape and position within the chamber.

The layout that provided the best performance in terms of the highest and most evenly distributed pressure over the surface substrate was a grated interface with a surface 2 mm from the high-vacuum region. Figure 9 displays results from DSMC calculations of the pressure in the environmental chamber under typical experimental conditions, with a grated interface separating the high-vacuum and high-pressure regions, seen from (a) the side and (b) the front. High and evenly distributed pressure over the surface substrate is essential to form and maintain a smooth condensed layer on the surface. However, high pressure may lead to transmission losses when beam molecules collide with background gas, thus the distance that molecules travel in the high-pressure region must be minimized. The closer the surface is to the high-vacuum region, the more difficult it is to maintain a high pressure over the surface. Thus, it is important to find the optimal distance where the pressure over the surface is sufficient and transmission losses are acceptable. The grating provides great improvement compared to, for example, a free opening since it reduces the potential pressure drop by a factor of three and leads to more

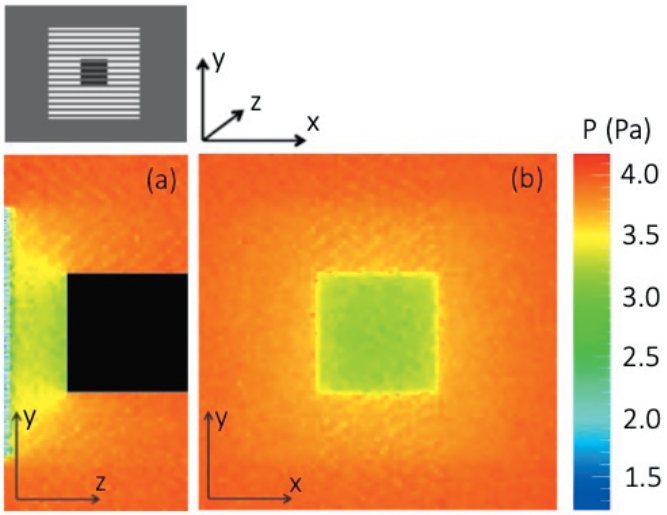

Figure 9. Results of DSMC simulations of the pressure in the environmental chamber with a grated opening from (a) the side and (b) the front.

evenly distributed pressure over the surface. Figure 10 shows the normalized pressure from DSMC calculations one grid cell above the

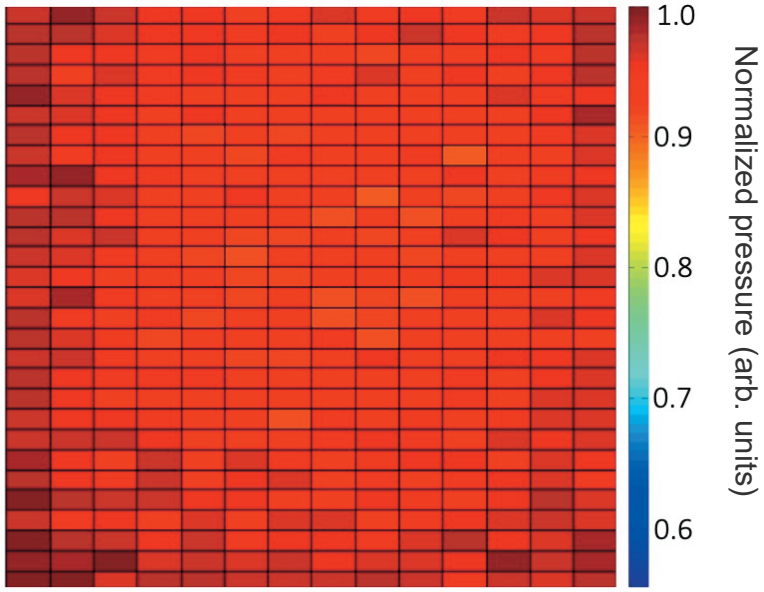

Figure 10. DSMC simulations of the normalized pressure over the surface with the new the grated interface and experimental layout.

surface substrate using a grated interface. This reduces the difference in pressures at the center of the surface and edges by more than a factor of four (to < 10%), compared to the difference with a free opening. The DSMC calculations indicate that the grated interface and new experimental layout expand the experimental pressure range and enable formation of smooth surface coatings during measurements.

The physical components were produced and the new layout was tested by using it in beam transmission experiments, in which a helium beam was directed onto the graphite substrate (kept at $T = 209$ K). The scattered flux was observed in the specular angle of the incident beam as water vapor was dosed into the environmental chamber. At this temperature and pressures water cannot condense on the graphite substrate, so a signal drop is solely due to beam collisions with background gas. Figure 11 displays the transmission of helium atoms in the high-pressure zone as a function of the experimental pressure. Results obtained using the EMB 3.0 setup, in

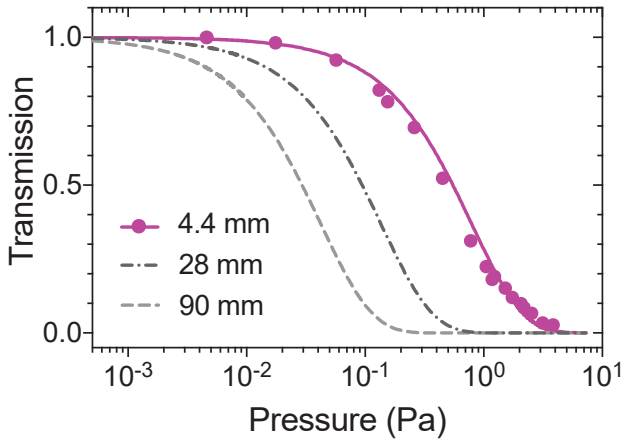

Figure 11. Helium beam transmission as a function of experimental pressure for EMB 3.0 (purple dots) and calculated transmission curves with three path lengths in the high pressure zone: 90, 28 and 4.4 mm (dashed grey, dash-dotted grey, and purple lines, respectively).

which the distance for molecules to travel in the high-pressure zone is 4.4 mm, are shown as purple dots. The experimental results were compared with the calculated transmission parameter T_P for EMB 1.0–3.0 setups using the Beer-Lambert law

$$T_P = e^{-Pl\phi}, \qquad \text{Eq. 2}$$

Here, P is the pressure, l is the molecular flight path in the high-pressure zone (l = 90, 28 and 4.0 mm in the EMB 1.0, 2.0 and 3.0 setups, respectively) and ϕ is the collision cross-section of helium and water molecules. As expected from the equation, reducing the distance for molecules to travel in the high-pressure zone shifts the transmission curves to higher potential experimental pressures. The transmission signal for EMB 3.0 starts to decline at around 10^{-1} Pa, and at 1 Pa 30% of the initial MB signal is transmitted. The transmission measurements clearly show that the EMB 3.0 setup provides improved performance than previous versions in terms of transmission at high experimental pressures.

4.2 Data analysis

The ToF distributions obtained during experiments were analyzed with a non-linear least squares fitting procedure in which the data were usually interpreted as a combination of two possible components, one related to inelastic scattering (IS) and one to thermal desorption (TD) of molecules from the surface. The result is a best fit of a convolution of the IS and TD components and the incident beam profile to the experimental data. The molecules that interact for the shortest time with the surface will arrive at the detector first. Molecules that are scattered inelastically from the surface subsequently reach the detector before the desorbing molecules, and the IS intensity profile can be modeled as a modified Maxwell-Boltzmann distribution,[45]

$$I_{IS}\big(v(t)\big) = C_i v(t)^4 exp\left[-\left(\frac{v(t)-\bar{v}}{\sqrt{\frac{2k_B T_{IS}}{m}}}\right)^2\right]. \qquad \text{Eq. 3}$$

Here C_i is a scaling parameter, v is the velocity related to the molecular arrival time, $\bar{v}$ is the average IS velocity, k_B is the Boltzmann constant, m is the mass of the MB molecule, and T_{IS} is the temperature spread of the IS component.

Molecules that are thermalized in contact with the surface and trapped there for some time before they desorb reach the detector later than the first IS molecules. The intensity profile of a TD component is explained as a convolution of two distributions, one that relates the TD velocity distribution to surface temperature,

$$I_{TDi}\big(v(t)\big) = C_j v(t)^4 exp\left[-\left(\frac{v(t)}{\sqrt{\frac{2k_BT}{m}}}\right)^2\right], \qquad \text{Eq. 4}$$

and one that relates desorption probability to the change in water population on the surface,

$$I_{TDj} = C_j e^{-kt}. \qquad \text{Eq. 5}$$

Here C_j is a scaling factor, T is the surface temperature, k is the desorption rate coefficient, and t is the detection time.

The non-linear least squares fitting of the IS and TD components to the experimental data was performed with numerical minimization of the residual between the total fit and the experimental data using five (or seven, when two desorption components were present) free fitting parameters. Three parameters reflect the amplitude (C_i), width (T_{IS}) and position ($\bar{v}$) of the IS component, and two represent the amplitude (C_j) and exponential decay (k) of the TD component. Figure 12 shows illustrative ToF distributions of (a) the D_2O beam and (b, c) D_2O fluxes from a graphite surface at $T = 200$ K. Figure 12c includes the fitted IS and TD components with an explanation of the five fitting parameters.

The temperature dependence of the desorption rate coefficient extracted from the fitting procedure can be related to the activation energy using the Arrhenius equation,

$$k = Ae^{\left(-\frac{E_a}{k_BT}\right)}. \qquad \text{Eq. 6}$$

Here A is a pre-exponential factor and E_a is the activation energy for thermal desorption. Eq. 6 can be reorganized as

$$\ln k = -\frac{E_a}{k_B}\frac{1}{T} + \ln A, \qquad \text{Eq. 7}$$

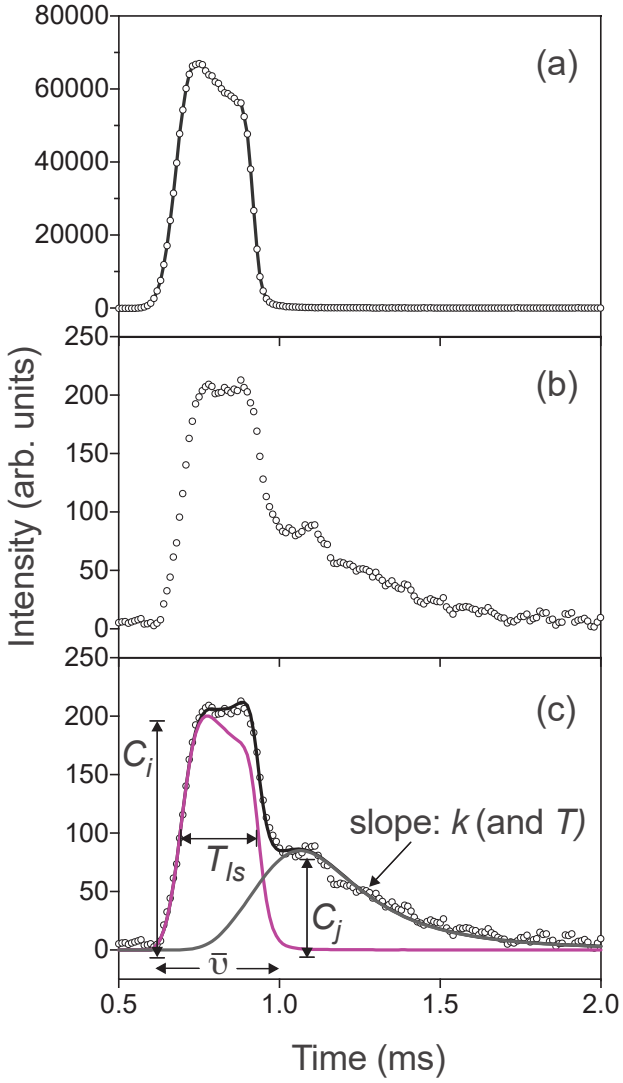

Figure 12. ToF distributions of (a) the molecular beam and (b and c) water fluxes from graphite at θ = 45°. The fitted IS (purple line) and TD (grey line) components and total fit (black line) are shown in (c).

and if ln k is plotted against $\frac{1}{T}$ it generates a straight line where the slope is proportional to E_a and the intercept with the y-axis is equal to ln A. The activation energy can also be calculated assuming that water undergoes first order desorption and has a typical pre-exponential factor of $A = 10^{13}$ s^{-1}.[46]

The angular molecular flux from a condensed layer can be described generally using a focused cosine function,

$$I_{TD/IS}^{x} = cos(\theta - \theta_{max})^{n}, \quad \text{Eq. 8}$$

where θ_{max} is the peak intensity angle with respect to the surface normal, θ is the observation angle, and n is a shape factor. Molecules that are thermalized in contact with the surface lose all their initial momentum and consequently desorb randomly in all directions. Thus, for the TD component θ_{max} = 0 and n = 1, which results in a typical cos(θ) distribution for TD. This makes the total integrated TD intensity I_{TD}^{x} easy to estimate by observing the molecular flux at any single observation angle. The absolute trapping desorption probability (P_{TD}) for water on a condensed phase x is obtained by comparing I_{TD}^{x} with TD from a clean graphite surface I_{TD}^{g} under similar conditions,

$$P_{TD} = \frac{S_g\, I_{TD}^{x}}{I_{TD}^{g}}, \quad \text{Eq. 9}$$

using a well-known sticking coefficient of water on graphite S_g = 0.73 ± 0.07.[15] The integrated IS intensity I_{IS}^{x} from a condensed layer is more difficult to estimate as it has a spatially directed flow related to the incident MB direction. The narrow IS flux may be explained using Eq. 8 with typical θ_{max} = 40–60 and n = 10–60. The total I_{IS}^{x} is quantified by assuming that scattering out of the plane, relative to the incident beam, has a similar angular profile as the in-plane scattering. The absolute inelastic scattering probability P_{IS} is obtained by normalizing I_{IS}^{x} to P_{TD}. The molecules that are trapped on the condensed surface for times exceeding the experimental timescale (10 ms) are assumed to be accommodated or sticking (a more strongly bound state than trapped) on the surface. A sticking coefficient α can be calculated from the IS and TD probabilities:

$$\alpha = 1 - P_{TD} - P_{IS}. \quad \text{Eq. 10}$$

4.3 Comparison with Molecular Dynamics simulations

Molecular Dynamics (MD) simulations were used in several of the studies reported in the appended papers to complement the experimental

investigations. These are computational simulations of the motions of atoms or interacting molecules (restricted by interatomic potentials or so-called 'force fields') in a system for a given time.[47] The dynamics of the molecules in the system are calculated by solving Newton's equations of motion for the system with the parameter set associated with the force fields. MD simulations have the advantage of high time resolution, as time steps of femtoseconds are commonly used. However, longer simulations result in high computational costs and time, so simulation run times rarely exceed microseconds. Due to the high time resolution of MD simulations, the outputs are not directly comparable with results of EMB experiments, but they may provide useful complementary indications of interactions between molecules that cannot be captured experimentally.

5. RESULTS AND DISCUSSION

This section presents and considers results of four studies on three systems, in which interactions between water and surfaces formed from a biogenic SOA compound, an alcohol, and a carboxylic acid, were probed in EMB experiments and complementary MD simulations.

5.1 Water interactions with a biogenic SOA compound (Papers II and IV)

Nopinone is one of the major primary products of β-pinene oxidation.[48–50] β-pinene is a VOC emitted by numerous plants (notably conifers). It is reactive and thus has a short lifetime in the atmosphere. Nopinone has a relatively high vapor pressure at room temperature, and has been found in both particle and gas phases in ambient and chamber experiments.[51–53] It has a melting point of 260 K,[54] so it may be present in both solid and liquid forms in the atmosphere. Nopinone ($C_9H_{14}O$) has a bicyclic hydrocarbon structure with an attached carbonyl group, and it is a fairly small but bulky molecule. MD simulations show that nopinone in a solid phase state (the one studied in the experiments reported here), forms bilayers of tilted nopinone molecules, with the carbonyl moieties directed into the bilayers (Fig. 13). Such layers expose few functional groups on the surface, which may lead to scarce opportunity for water to bind in strongly.

The experimental results, however, show that molecularly thin nopinone layers coating graphite and micrometer-thick nopinone layers have high ($\geq$ 97%) water trapping efficiency. This is a result of efficient energy transfer in the collisions that results in weak interactions between water and the hydrocarbon structure in the nopinone framework. Accordingly, light scattering during the condensation process indicate that the micrometer-thick layers formed during the experiments may be polycrystalline, something that has been observed before.[40] A polycrystalline surface may contain surface defects and grain boundaries where functional groups are easily accessible for water to bind to. In the experiments, thicker layers can be maintained up to 220 K, and thin layers of nopinone coating

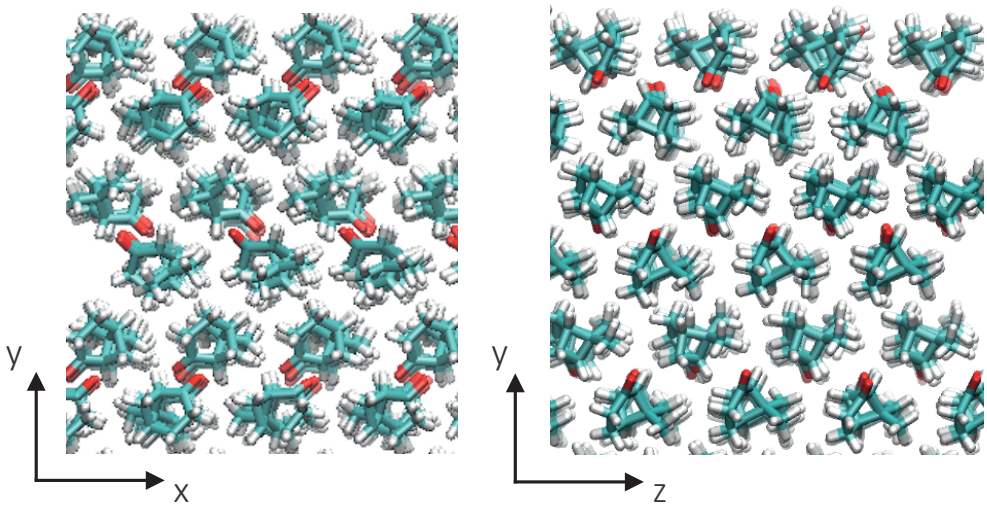

Figure 13. Snapshots of a nopinone crystal from MD simulations seen from two sides of a simulation box. The figure is included in this thesis with permission from Josip Lovrić.

graphite have been generated for high temperature measurements (200–270 K). The thin nopinone coatings may consist of a monolayer or a few bilayers. Their exact thickness cannot be determined due to limitations in the optical equipment's resolution. However, the thin layers are much more stable than the micrometer-thick layers, indicating that they are structurally different from the thicker layers. Another indication that the micrometer-thick layers and molecularly thin coatings may be slightly different is that the absolute TD efficiency from them significantly differs. A reduction in TD probability on thin coatings compared to micrometer-thick layers may be caused by a change in molecular density. Such densification of thin coatings has preciously been observed for thin layers that induce higher 2D ordering relative to thicker layers.[55] However, the main processes observed on the nopinone surfaces are still the same.

ToF distributions obtained from the QMS were analyzed and fitted with IS and TD components using the procedure detailed in the methodology section. Figure 14 shows two fitted ToF distributions of water intensities as a function of time measured from a nopinone coating on graphite at $T = 270$ K in different directions with respect to the surface normal. The IS component is low in directions close to the surface normal, and is mainly

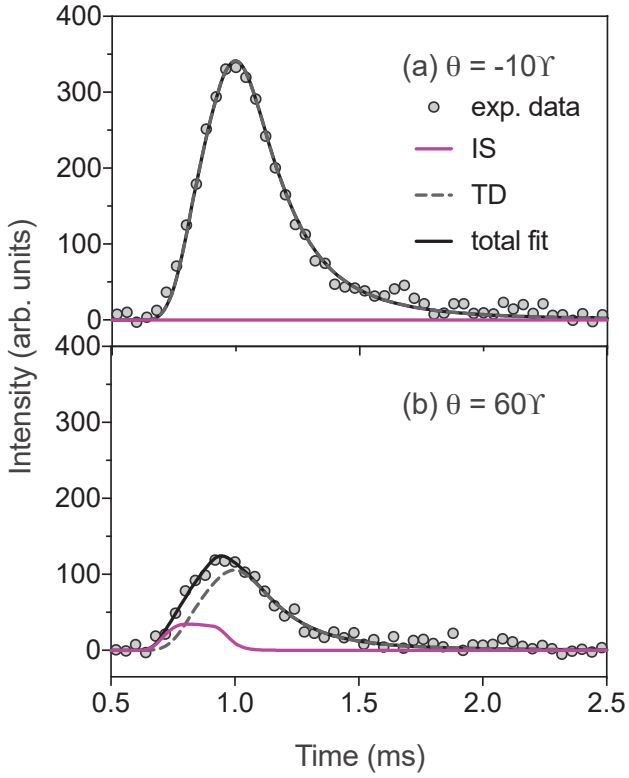

Figure 14. ToF distributions of water intensities from a thin nopinone layer coating graphite at T = 270 K as a function of time at observation angles of (a) -10° and (b) 60°. Fitted IS (purple line) and TD (grey dashed line) components and the total fit (black line) are superimposed on the experimental data (circles).

detected around the specular direction. The IS profile is similar to the incident beam profile and is merely broadened and delayed due to efficient energy transfer (35–80%) in surface contact. This compares well with results from EMB studies of other water-organic systems.[56–60,15] Most of the intensity flux is associated with molecules that are thermalized in the interaction with the surface and then desorb. The short 'tail' of the TD velocity distribution indicates that the desorption process is fast (actually in this case faster than the time resolution of the experimental method). Hence, we can say that most molecules spend less than 10 μs on the surface before they desorb. The observed desorption rate coefficient $k \geq 10^5$ s^{-1}, and these rapidly desorbing molecules must experience binding

energies weaker than 26 kJ mol^{-1} (calculated energy at the lowest employed experimental T = 170 K) before they desorb. These molecules may potentially encounter and bind to carbonyl moieties available on the surface or interact weakly with the nopinone hydrocarbon structure before desorption.

The IS and TD components can be integrated for each observation angle and plotted as angular distributions (Fig. 15). In the Figure, the IS component has been multiplied by a factor of ten to increase its visibility, so it is only a minor component of the total flux. The Figure shows that the IS angular distribution is rather narrow and reaches a peak around the

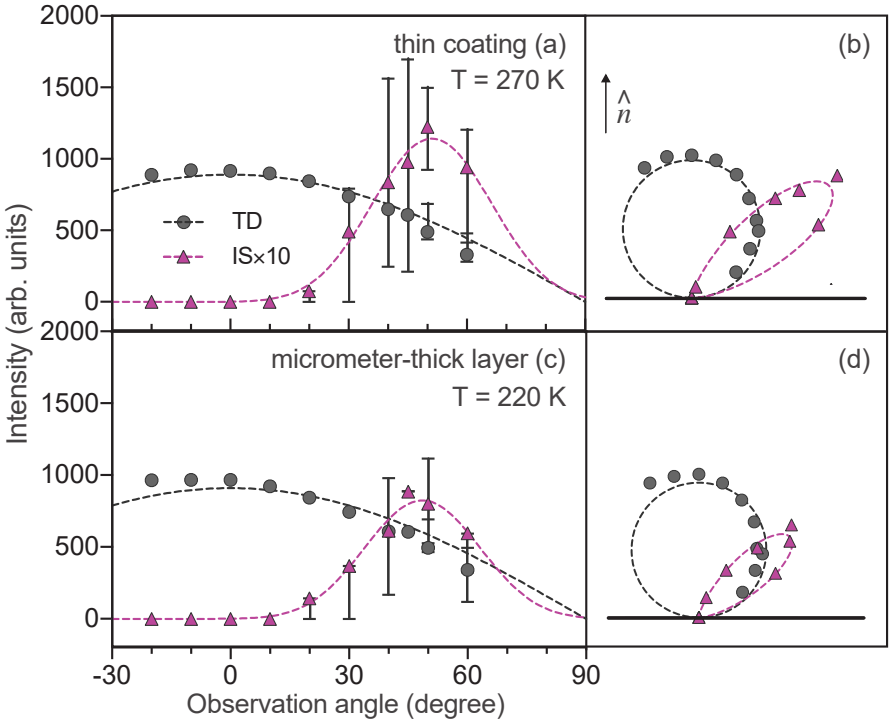

Figure 15. Angular distributions of water from a thin nopinone coating on graphite at 270 K (a and b), and a micrometer-thick nopinone layer at 220 K (b and c). The right hand side shows polar plots of the angular distributions shown to the left.

specular angle of the incident beam. There is no significant difference in angular scattering trends for a molecularly thin nopinone coating on graphite and a micrometer-thick nopinone layer. This indicates that local surface roughness may be present in both cases. There is also little

difference in probability of TD between the two types of surfaces. Clearly, as molecules are thermalized on the surface they lose all 'memory' of their incident trajectory before surface contact and desorb with equal likelihood in all directions. This generates a typical cosine distribution for the TD process.

A fraction of the impinging water molecules form stronger bonds with the surface and do not desorb within the experimental time window (10 ms). These molecules, which we do not observe desorbing, must have a desorption rate coefficient $k \leq 10^2$ s^{-1} and interact with surface-bound molecules with binding energies exceeding 57 kJ mol^{-1} (at T = 270 K). Such molecules may have diffused rapidly on the surface and encountered other water molecules that they may bind to and hence interact with stronger binding energies. Similar rapid diffusion patterns have also been seen in EMB studies of methanol-graphite systems.[61] Figure 16 shows the sticking coefficient (α), which ranges from 20 to 40% and is slightly

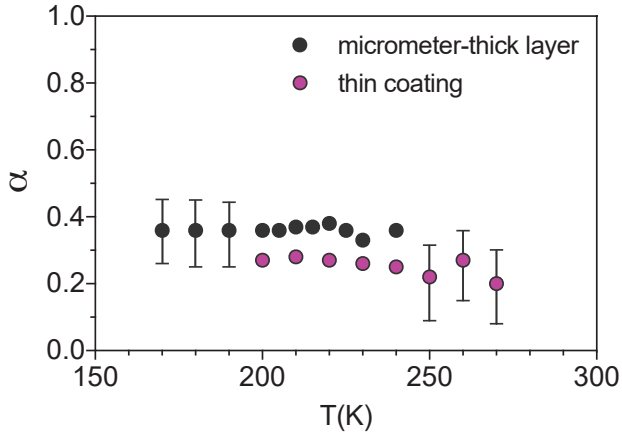

Figure 16. The accommodation coefficient as a function of temperature for micrometer-thick nopinone layers (black dots) and thin nopinone coatings on graphite (purple dots).

higher for micrometer-thick nopinone layers than for thin coatings of nopinone on graphite. This may, as mentioned earlier, be related to that a molecularly thin layer may be denser than the micrometer-thick layer, which makes functional groups within the thin layer less accessible for water. α does not seem to have clear temperature dependence, at least not

in the investigated temperature interval. No water coating has been observed to gradually build up on the nopinone surface. Thus, the succeeding desorption process must be so slow that it is not observed in the experimental window, but fast enough to desorb between beam pulses and contributing to the background levels.

To summarize, investigated nopinone surfaces show high water trapping probabilities (≥ 97%). A majority of the water molecules may interact with the hydrocarbon structure or carbonyl groups on the nopinone surface with weaker binding energies (≤ 26 kJ mol^{-1}) followed by fast desorption (≥ 10^5 s^{-1}). A minor fraction may interact with other surface bound water molecules and form stronger bonds (≥57 kJ mol^{-1}) and contribute to the sticking coefficient (20–40%). Micrometer-thick nopinone layers showed increased propensity to accommodate water compared to thin nopinone coatings on graphite, something that potentially may be related to structural differences in the different layers.

5.2 Water interactions with an alcohol (Paper III)

Alcohols are common oxidation reaction products and primary components of VOC emissions in the atmosphere. Straight-chained primary alcohols may act as surfactants as their hydroxyl groups are hydrophilic and their carbon chains are hydrophobic. Thus, they can coat aerosol particles and create a barrier that limit transport of water and other trace gases into aerosol particles.[62,10] In our EMB study, *n*-butanol was chosen as a proxy for the diverse alcohols present in the atmosphere. It was regarded as an optimal surface molecule for this purpose as it has a suitable vapor pressure and melting point for low temperature EMB studies. The melting point (184.5 K) enables investigations of water interactions with both solid and liquid *n*-butanol surfaces.[63] Results from MD simulations of the relaxation of a *n*-butanol crystal at low temperature indicate that the solid crystal is composed of bilayers of tilted *n*-butanol molecules connected at their hydroxyl groups (Fig. 17a). In contrast to the nopinone crystal structure, where the bulkiness of the nopinone molecule restricts the molecules in an ordered arrangement throughout the whole slab, tails of the *n*-butanol molecules in the upper layer of the crystal are

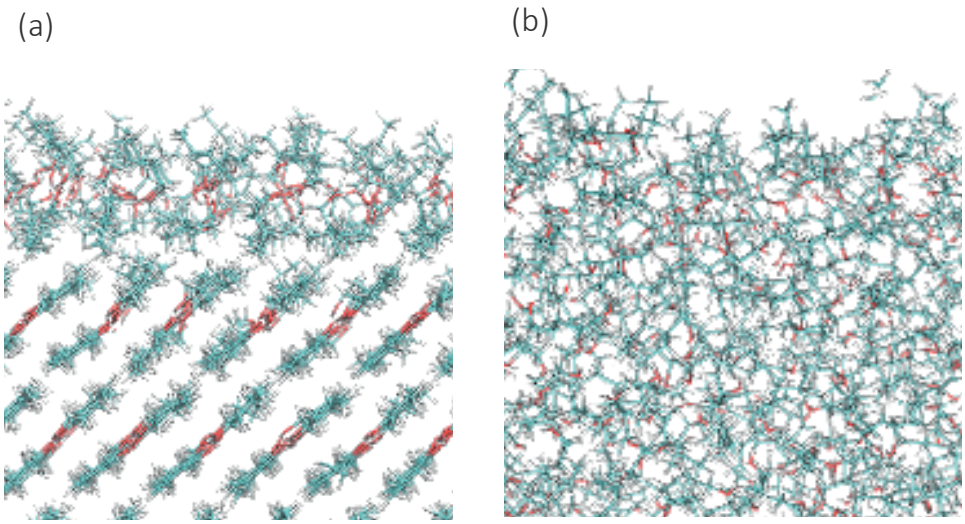

Figure 17. Snapshots of (a) solid and (b) liquid *n*-butanol slabs generated from MD simulations. The figure is included in this thesis with permission from Josip Lovrić.

fairly mobile, generating the disordered surface depicted in Figure 17a. Naturally, the molecular mobility and disordering spread to the whole slab as the crystal melts (Fig. 17b).

Paper III presents results from water-butanol EMB experiments together with a re-analysis of results of a previous EMB study of a similar system.[57] Analysis of the new results, which included more information from the angular flux profile, clearly indicated that the water flux from solid *n*-butanol surfaces cannot be modeled with only one IS and one TD component. Instead two TD components with significantly different desorption rate coefficients had to be included. This is not obvious when observing the flux in the specular angle (as in the earlier study), but is clarified with information from different observation angles, especially around the surface normal direction where TD dominates the flux.

Figure 18 shows ToF distributions from a solid *n*-butanol surface in two directions with respect to the surface normal, and fitting lines for one IS component and two (TD_{fast} and TD_{slow}) TD components. As in the studied water-nopinone systems, the rapidly desorbing molecules spend a short time on the surface before desorbing, shorter than the resolution of the

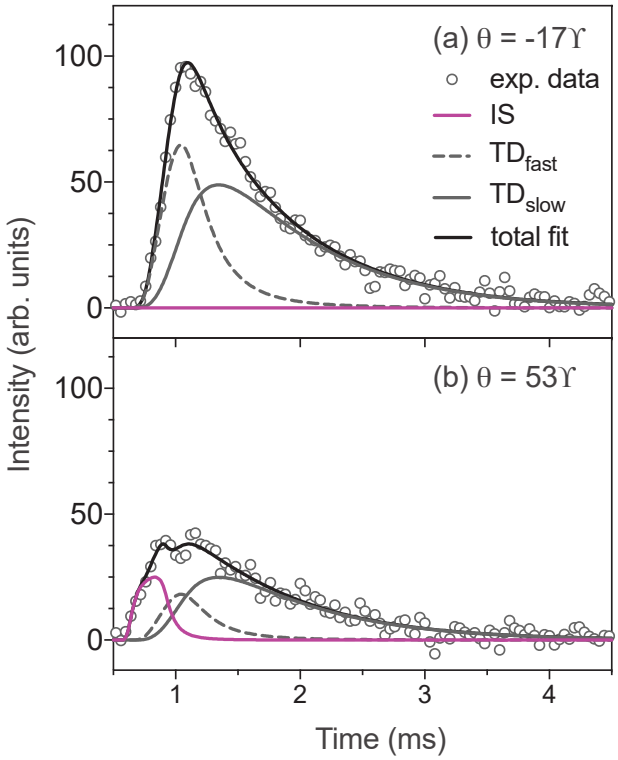

Figure 18. ToF distributions of water flux intensities from a solid *n*-butanol layer at T = 179 K as a function of time at observation angles of (a) -17° and (b) 53°. Fitted IS (purple line), fast TD (grey dashed line) and slow TD (grey solid line) components along with total fit (black line) are superimposed on the experimental data (circles).

experimental method. Thus, the TD_{fast} rate coefficient $k \geq 10^5$ s^{-1}. The temperature dependence of the TD_{fast} rate coefficient is masked by the temporal resolution of the technique, so only an upper limit of the activation energy for desorption can be determined ($\leq$ 27 kJ mol^{-1} at T = 179 K).

The TD_{slow} component, which is mainly observed in experiments with solid surfaces, has resolvable desorption rate coefficients that varies, with temperature, in the range $k = 5\times10^2$–1.3×10^3 s^{-1}. Molecules contributing to this component spend a few milliseconds on the surface, which may be related to activation energies of 34–37 kJ mol^{-1}. These more strongly bound molecules desorb from solid and pre-melted *n*-butanol surfaces,

while on liquid surfaces the slow component is not apparent. This indicates that if water molecules bind more strongly to the liquid *n*-butanol layer they are likely incorporated into the highly mobile surface.

Angular distributions of IS (multiplied by a factor) and TD components from solid (Fig. 19a and b) and liquid (Fig. 19c and d) *n*-butanol differ most strongly. There are clearly two TD components (TD_{fast} and TD_{slow}) from solid surfaces, but only the TD_{fast} component from the liquid surfaces. The IS component is broad in both cases, indicating that (like the liquid surface) the solid surface is locally disordered. Inelastically scattered molecules lose 60–90% of their initial kinetic energy in the interactions with the surface.

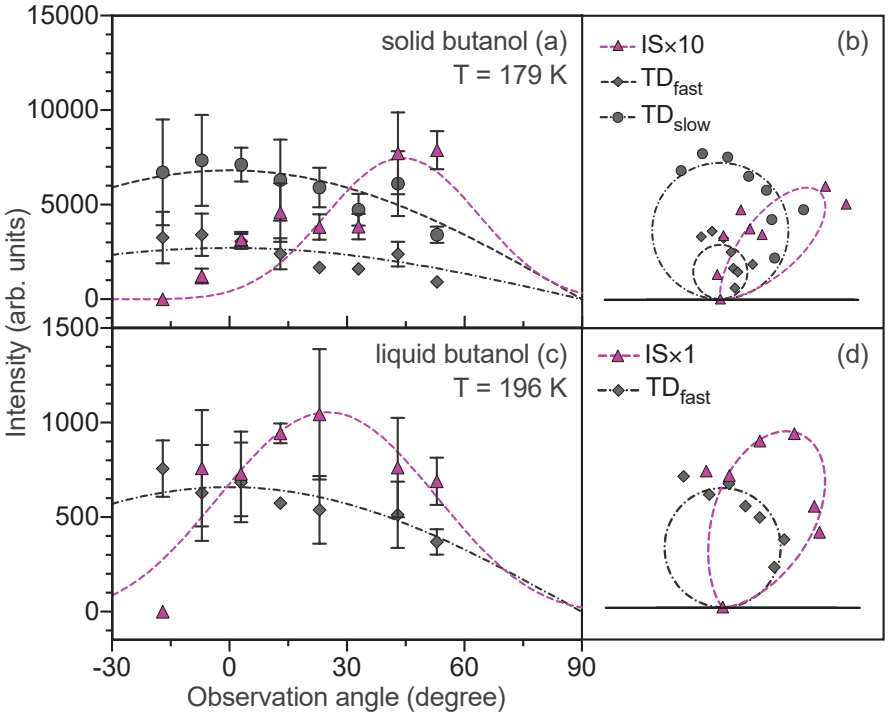

Figure 19. Angular distributions of integrated water intensities from a solid *n*-butanol layer at 179 K (a and b), and liquid *n*-butanol layer at 196 K (c and d). The right hand side shows polar plots of the angular distributions shown to the left.

The IS probability is low at all investigated temperatures, but the TD probability changes dramatically as the surface properties change (Fig.

20a). The total TD probability increases with temperature from 0.65 to unity for solid surfaces, but within a 10 K window around the melting point it dramatically declines and stabilizes at ≈ 0.2 for liquid surfaces. Figure 20a highlights the fact that the TD_{slow} component disappears completely on liquid *n*-butanol surfaces. The upper layer of the *n*-butanol crystal melts gradually and the layer is not fully melted until a few degrees above the melting point, which strongly influences the desorption behavior. MD simulations confirm the gradual melting of bulk *n*-butanol.

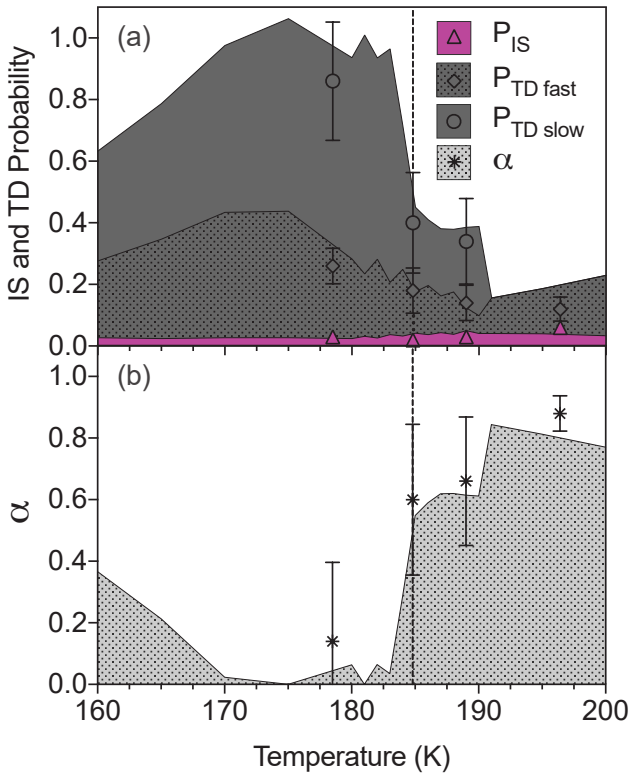

Figure 20. (a) IS (purple triangles), TD_{fast} (grey diamonds), TD_{slow} (grey circles) probabilities and (b) the sticking coefficient (black stars) as a function of temperature on solid and liquid *n*-butanol surfaces. The results are superimposed onto the re-analyzed results from a previous study by Papagiannakopoulos *et al.* shown using the shaded regions. The dashed line shows the experimentally determined melting point.

At most test temperatures a fraction of molecules form strong bonds that make them stick on the surface for times longer than the measurement

time (10 ms), as observed in the water-nopinone study. These molecules, which we do not observe desorbing, have a desorption rate coefficient of $k \leq 10^2$ s^{-1} and interact with the surface with binding energies stronger than 41 kJ mol^{-1} (at T = 196 K). The sticking coefficient, which represents the probability for strongly bound molecules, is displayed in Figure 20b. The probability for molecules to stick on solid surfaces is low, but as the *n*-butanol layer gradually melts α increases to about 0.8. This shows that gas-surface interactions are strongly influenced by the viscosity of the surface. Therefor, sticking coefficients for liquid surfaces cannot be reliably obtained by monitoring interactions with solid phases and extrapolating the observed behavior to higher temperatures.

The minor deviation between the results from the current study (data points) and previous study[57] (shaded areas) in Figure 20 may be due to the new study providing an overall view of the IS and TD processes through the angular-resolved observations, while the previous study was limited to a single observation angle (specular angle, 45°). In addition, the normalization to the total intensity was improved in the new study, and the poorer normalization may explain why some of the previous TD probability values exceeded 100%.

To conclude, the thermal desorption scheme on *n*-butanol surfaces is complex and cannot be explained by a single TD component, but is in fact comprised by two (TD_{fast} and TD_{slow}) components. The TD_{fast} channel is made up by rapidly desorbing molecules with activation energies ≤ 27 kJ mol^{-1}, and the TD_{slow} channel consists of molecules that are more strongly bound (34–37 kJ mol^{-1}) and spend a few milliseconds on the surface before desorbing. The desorption scheme is highly influenced by the phase state of the *n*-butanol layer and the total TD probability is high for solid surfaces (65–100%) and significantly lower for liquid layers (20%). Thus the sticking coefficient varies with temperature (0–80%).

5.3 Water interactions with a carboxylic acid (Paper V)

Carboxylic acids are common primary and secondary reaction products of natural processes emitted to the atmosphere.[26] Valeric acid is a five-carbon straight-chained carboxylic acid, also called pentanoic acid, with a melting

point of 240 K.[63] Since temperatures in EMB water-valeric acid experiments were between 170 and 220 K, the experimental surfaces consisted of solid crystals. MD simulations indicate that solid valeric acid crystals consist of parallel layers of horizontally arranged molecules (Fig. 21), in which each valeric acid molecule binds to another, forming dimers that lie flat on the surface with functional groups exposed. The valeric acid molecules' formation of stable dimers reduces their functional groups' availability for water to bind and form strong binding sites.

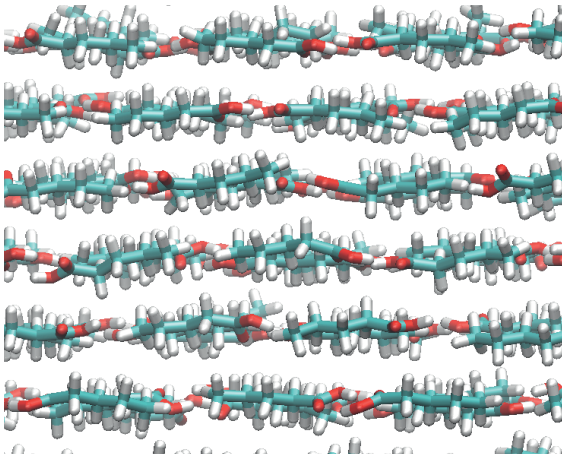

Figure 21. A snapshot of a solid valeric acid slab generated from MD simulations. The figure is included in this thesis with permission from Josip Lovrić.

A majority of water molecules impinging on thin valeric acid coatings on graphite and micrometer-thick valeric acid surfaces in the EMB experiments were thermalized in contact with the surface. Only 2±1% were scattered in the interaction, losing 50–80% of their kinetic energy in surface contact. Most (65–85%) molecules trapped on the surface desorbed within the first 10 μs, and thus had an unresolved desorption rate coefficient $k \geq 10^5$ s^{-1}. However, the fluxes also included a small fraction of slowly desorbing molecules. Figure 22 displays the water flux in the normal direction from a micrometer-thick layer of valeric acid at 160 K. During the analysis it became apparent that two desorption components (Fig 22a) were needed to fit the flux, not just one (Fig 22b). Commonly we have observed one-component desorption,[64,65] but in some cases, like this and the water-butanol study, the flux cannot be fitted with one component

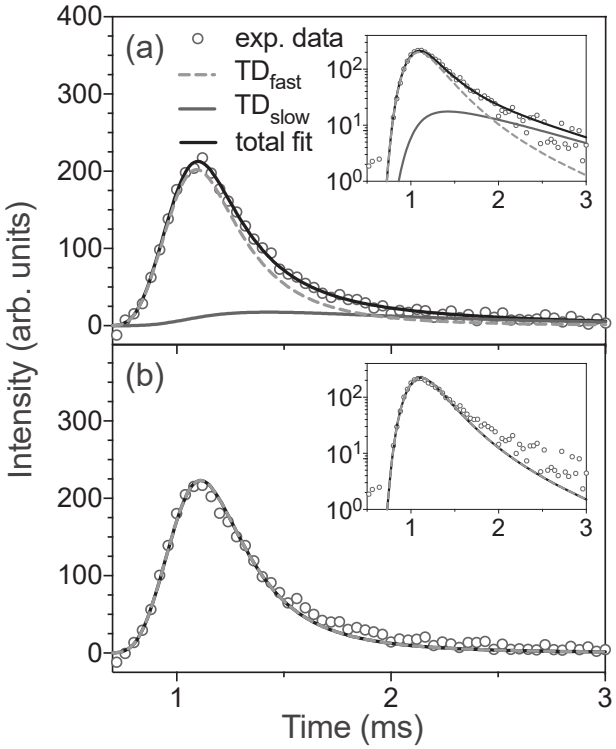

Figure 22. ToF distributions of water intensities observed in the normal direction from a micrometer-thick valeric acid layer at T = 160 K, in normal and log scale (insets). The TD_{fast} and TD_{slow} components (grey solid and dashed lines respectively) and total TD (black line) are displayed together with the experimental data (circles). (a) and (b) show fitted fluxes with two and one TD component, respectively.

and is better explained by two TD components.[60] The minor TD_{slow} component was more prominent in experiments with cold surfaces, where the TD_{slow} rate coefficient was higher compared to high temperature surfaces (total range 4.5×10^{2}–1.5×10^{3} s^{-1}). The molecules involved spend on average 0.5–2.5 ms on the surface before desorbing and contribute with 5–20% of the total flux.

The activation energy of desorption can be estimated from an Arrhenius plot (Fig. 23), where the y-axis intercept is equal to the pre-exponential factor, which as mentioned earlier is often assumed to be $\approx 10^{13}$ $s^{-1}$for water, and the slope is related to the activation energy. However, the shallow slope of the trendline for TD_{slow} in Figure 23 indicate that the temperature dependence is rather weak and the intercept with the y-axis is

far from the value one may assume of $\ln(10^{13})$. The observed negative temperature dependence of the TD_{slow} desorption coefficient is also an interesting feature. These observations indicate that the slow desorption process is complex, and is likely to occur via several steps.

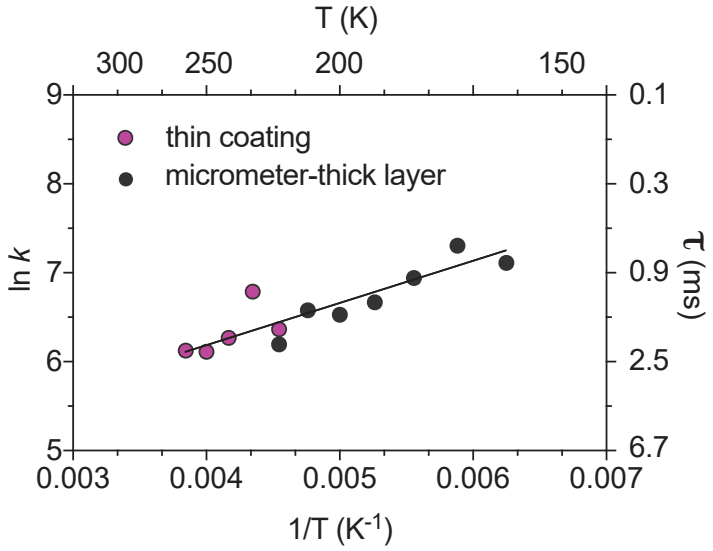

Figure 23. Arrhenius plot showing the temperature dependence of the TD_{slow} rate coefficient. The purple and black dots represents water desorption rates from thin valeric acid coatings on graphite and micrometer-thick valeric acid layers respectively.

MD simulations suggests that local surface disordering increase with increasing temperature. This means that the potential for impinging water to diffuse on the surface and find dirsordered areas with exposed funtional groups becomes more liklely with an increase in temperature. Interactions with functional groups results in higher binding energies and longer residence time (τ) on the surface, relative to the weaker interactions with the valeric acid hydrocarbon structure. Thus this increased potential for water to form stronger bonds with valeric acid functional groups on high temperature surfaces may explain the negative temperature dependece of the TD_{slow} rate coefficient. The observed TD_{slow} desorption coefficient is really a combination of rate coefficients for desorption and preceding diffusion and strongly bounded steps.

As in water-nopinone systems, there is a difference in water uptake between thin valeric acid coatings on graphite and micrometer-thick layers (Fig. 24). However, in contrast to the pattern observed in the nopinone study, for valeric acid more water sticks to the thin coatings than the thicker surfaces. The exact structure of the thin coatings of valeric acid on graphite has not been established, so it is uncertain if dimer formation also occurs in them. If the low surface coverage of valeric acid on graphite does not result in dimer formation, the functional groups will be more accessible for water to bind strongly with, which may explain the higher sticking coefficient. The thin coatings are more stable than the thick layers, so they are likely to have different structure, but the EMB experiments provide no further structural information.

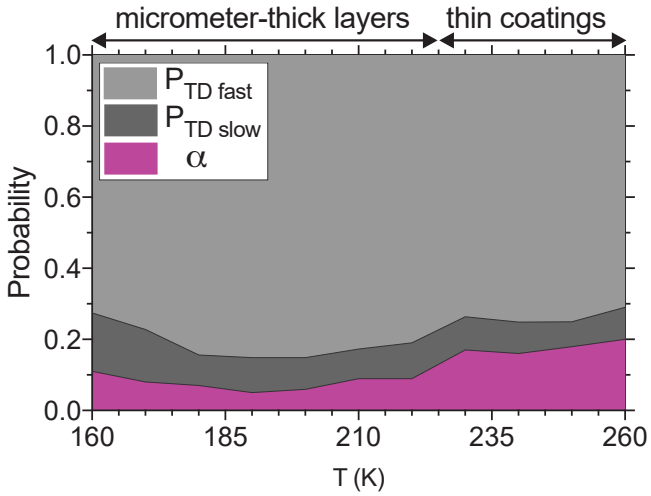

Figure 24. TD_{fast} (light grey), TD_{slow} (dark grey) and α (purple) probabilities as a function of temperature on micrometer-thick layers and thin valeric acid coatings on graphite.

However, the overall scattering and desorption trends observed with different valeric acid surfaces across the experimental temperature interval are consistent. Angular distributions of IS×10 and total TD componetns in water fluxes from a thin valeric acid coating on graphite at 260 K are shown in Figure 25a and b, and corresponding distributions obtained in experiments with a micrometer-thick valeric acid layer at 220 K in Figure 25b and c. The total desorption component agrees well with a cosine

distribution and the scattering component is narrow, with a maximum around the specular angle of the incident beam, in accordance with patterns observed in other water-organic interaction studies.[65,60,43]

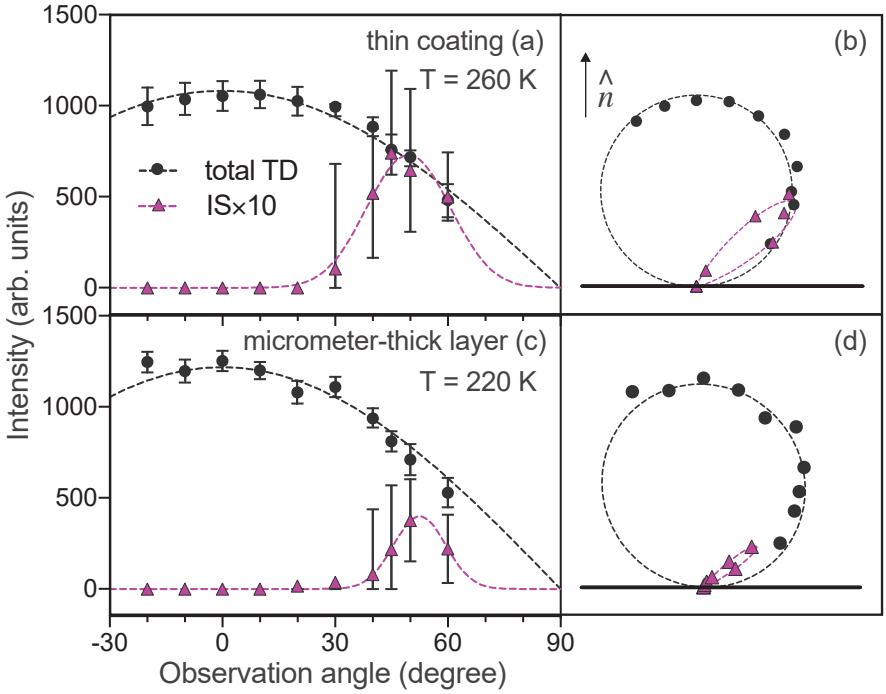

Figure 25. Angular distributions of water fluxes from a thin valeric acid coating on graphite at 260 K (a and b), and micrometer-thick valeric acid layer at 220 K (c and d). The right hand side shows polar plots of the angular distributions shown to the left.

In summary, the water trapping efficiency of valeric acid surfaces is high (≥ 97%), and the succeeding desorption process is complex consisting of two TD compoents. Rapidly desorbing molecules (65–85%) spend ≤ 10 μs on the surface before desorption, while the slowly desorbing molecules (5–20%) stay on avergae 0.5–2.5 ms on the surface. Local surface disordering may be enhanced on warm surfaces facilitating rapid diffusion to stronger binding sites, relative to cold surfaces. This is a possible explanation to the negative temperature dependence of the observed TD_{slow} rate coefficient. The sticking coefficient varies between 5 and 20%, and

differs slightly for thin valeric acid coatings on graphite compared to micrometer-thick valeric acid layers.

5.4 A comparison of water-organic systems

In this thesis I present work from studies of interactions between water and different organic systems: a biogenic SOA compound, an alcohol and a carboxylic acid. The results have provided interesting insights. To validate them and extend conclusions they should clearly be compared to other similar systems. However, there are only a limited number of similar experimental studies on the detailed kinetics and dynamics of water-organic systems. Hence the comparison is mainly focused on previous EMB studies, which include water-methanol,[56] water-hexanol,[58] water-acetic acid,[59] water-organics coated ice and water-ice systems.[15,58,14]

Due to the high incident kinetic energy of the MB molecules, fluxes coming from the experimental surface usually consist of a minor fraction of inelastically scattered molecules. A major fraction of molecules adsorb to the surface and subsequently desorb. The scattering component is highly dependent on the immediate environment of the surface for impinging molecules. In most cases this leads to the molecules losing a large fraction (30–90%)[56–59,15] of their initial kinetic energy, but maintaining some energy to scatter. In studies with solid and liquid surfaces we have seen comparable scattering channels. The scattering component is interesting in EMB experiments as it gives some information about surface structure and collision dynamics. However, it is less relevant for atmospheric systems where most water-aerosol surface interactions involve lower incident kinetic energies compared to the experimental ones.

Both recent and previous EMB studies indicate high trapping probabilities ($\geq$ 94%) for water on organic surfaces. In some systems, such as water-butanol,[60] water-hexanol,[58] water-acetic acid[59], water-nopinone,[65,43] and water-valeric acid[66] systems the adsorption process is followed by too rapid desorption ($k \geq 10^5$ s^{-1}) for resolution with the experimental setup. Sometimes adsorption is followed by slower resolvable desorption processes, as in water-methanol,[56] water-butanol[60] and water-valeric acid[66] systems. These observed components do not extend beyond the

experimental time window and their rate coefficients may be resolved. In a few cases, e.g. water-butanol[60] and water-valeric acid[66] systems, multi-component processes dominate the desorption flux. Here more than one TD channel is required to describe the water flux from the organic layers.

Surface properties such as chemical composition with potential availability of functional groups and polycrystallinity contributing to surface roughness and grain boundaries where water can bind seem to be important for water uptake. The availability of functional groups on surfaces will contribute to the surfaces' potential to accommodate water, so surfaces with low accessibility of functional groups due to dimer formation or the molecular orientation may have relatively low propensity to take up water. The density of the surface layer also reportedly to potentially affect the water accommodation process.[43] The phase state of the surface is another important factor, as desorption may be dramatically lower in liquid than in solid systems.[60] Most EMB studies are, however, performed with solid surfaces and we need to be aware of the difficulties of extrapolating the results to high temperature surfaces.

Collectively, desorption rate coefficients obtained for water-organic systems are higher than those obtained for water-ice systems in similar conditions. The process of desorption from ice surface occurs over a longer time scale, with sticking coefficients ranging from 0.5 to 1.0 for temperatures between 170 and 200 K.[14] Thus, the sticking coefficients are comparable to those of water-organic systems. Several studies have shown that organic coatings on ice may also cause changes in water uptake processes from those of pure ice surfaces.[67,13,16,15,58,14] Organic coatings may induce a significant increase in the desorption rates relative to ice surfaces, which can lead to a change in the total accommodation of water.[58,59] Some organics, such as methanol, *n*-butanol and *n*-hexanol, seem to be relatively permeable for water transport whereas other such as acetic acid trap water more efficiently.[15,58,59]

Both the studies that this thesis is based upon and previous EMB studies have shown that water uptake by organic surfaces may significantly depend on the chemical and physical properties of the organic layer. Thus,

researchers should be aware of these effects when trying to model interface processes in water-organic systems in the atmosphere.

6. CONCLUDING REMARKS

The thesis presents improvements to EMB methodology and results of evaluations of the new grated high-vacuum/high-pressure interface. The improvements have extended the experimental pressure range up to 1 Pa and enabled angular-resolved measurements. The EMB technique now have unparalleled capacity to explore the dynamics and kinetics of molecular interactions with volatile surfaces, and thus contribute to understanding of interfacial processes on atmospherically relevant surfaces.

The improved EMB methodology has been used to study molecular-level interactions between water and surfaces individually composed of three organics: a ketone (terpenoid), an alcohol and a carboxylic acid. These compounds have been selected as proxies for compounds that are frequent components of atmospheric SOA.

The investigations showed that the experimental surfaces show water trapping probabilities close to unity, and accommodate water to varying extents. We saw that desorption kinetics are influenced by the presence and accessibility of functional groups on the organic surfaces. The desorption process differs from thin organic coatings compared to micrometer-thick layers, something that may have to do with layer density and the accessibility of functional groups on the surface. The thick layers are likely polycrystalline and may present surface defects and grain boundaries where accessible functional groups facilitate strong water bonding. Water molecules likely diffuse rapidly on the organic surfaces and may find other water molecules, which also induce stronger binding and longer residence times. The phase state of the organic surface plays a major role in the sticking probability where strongly bound molecules cannot desorb from liquid layers. Sticking coefficients were found to range from 5 to 40% on solid surfaces and up to to 80% on liquid surfaces.

7. FUTURE PERSPECTIVE

The EMB experimental technique is useful for detailed studies of the dynamics and kinetics of gas-surface interactions. It has unparalleled capacities for investigations of molecular-level interactions between gases and volatile solid and liquid surfaces in required UHV experimental conditions. This makes it highly attractive for studying trace gas uptake on surfaces with a finite vapor pressure. Water is interesting because of its general importance in atmospheric systems, but there are other interesting gases. For example, uptake of other organics by organic systems warrants attention. Similarly, diverse organics could provide suitable surfaces for EMB experiments, depending on the objectives. Further explorations of interactions with condensed layers of a single type of molecule, such as a branched carboxylic acids, ester or diol would be valuable, as would experiments with mixtures of organics, such as real SOA samples. However, experimental restrictions related to contamination of the UHV system may limit the possibility of using too ‘sticky’ compounds, and thus should be considered.

When considering complex surface mixtures, questions regarding surface composition and properties immediately arise. Of course, these are pertinent in all EMB experiments, but they become more important if the surface substrate contains a mixture of compounds. What is the surface like? Do some compounds migrate to and accumulate at the gas-surface interface, or is the mixture homogeneous throughout the condensed layer? Addition of some type of spectroscopic analysis of real-time chemical composition would be highly advantageous, but difficult with current experimental setups.

ACKNOWLEDGEMENTS

Jan - Thank you for giving me the opportunity of working in your group. I've enjoyed it all; the time working in the lab developing the experimental setup and generating results, the analysis and discussions of the results and producing the scientific text. Experiments rarely go as one expects, but that's also the beauty of research, not knowing the outcome. If there's one thing I've learned it is to be patient and to keep an open and analytical mindset. I think that these are useful traits for future academic work as well as personal life, and for this experience I'm very grateful.

Kong and Erik - You've both been the foundation and support that I've felt that I can lean on when it comes to everything from advice in experimental procedure to guide me in scientific writing. We've had many interesting discussions and I've learned so much from you. Thank you.

Mattias - Thank you for your support and guidance, and for all fun discussions during lunch and fika breaks.

Johan - It's been nice to know that your door's always been open for discussions of small or large problems that have arisen during my PhD studies. Thank you.

Josip - and other co-authors, thank you for nice collaborations.

Atmospheric Science group - Dimitri, you're the best office roommate ever, even though your messiness (that you blame on the strive towards maximum entropy) is all over the place. I've enjoyed the fun sarcastic tone in the office, and of course the morning coffees and cookies. Atmochicks: Anna, Julia and Ågot - us girls have each others back. Although I only have brothers in real life, I feel like I've also got sisters now. Sisters of science, that's PP! A special thanks to Anna for proof reading this thesis, I know how tedious it is. Christian and Nondas, who needs girls in the group when one can come chat to you guys!? Thanks for your friendly and happy attitude. A big thank you to all other present and previous PhD students and post docs in the group, you have all contributed to making my time in the group joyful!

Family and Friends - I could never have made it this far without my family and friends. Thank you for your never-ending love and support!

Sepideh - Gummaaaaaan, you're the best! It feels like forever since I first met you in the Atmospheric Science group during the bachelor thesis work. We've come a long way together and you've always been my number one supporter. I'm so grateful for that. I'm also excited that I, with you by my side, get to explore one of life's greatest adventures in a very near future.

Dello - You're the voice of logics. Where would I be without you? Most likely I'd be lost in a sea of irrationally based decisions. I know that deep down you love science and that you're actually jealous of my work (even though you'd never admit that). So, as you would say, let's come together to trick the world!

REFERENCES

1. Seinfeld, J. H.; Pandis, S. N., Atmospheric Chemistry and Physics, from Air Pollution to Climate Change. *J. Atmos. Chem*. **2006**, 37 (2), 212-214.

2. Shrivastava, M.; Cappa, C. D.; Fan, J.; Goldstein, A. H.; Guenther, A. B.; Jimenez, J. L.; Kuang, C.; Laskin, A.; Martin, S. T.; Ng, N. L. *et al.*, Recent Advances in Understanding Secondary Organic Aerosol: Implications for Global Climate Forcing. *Rev. Geophys*. **2017**, 55 (2), 509-559.

3. IPCC, **2013**: Climate Change 2013: The Physical Science Basis. Contribution of Working Group I to the Fifth Assessment Report of the Intergovernmental Panel on Climate Change [Stocker, T.F., D. Qin, G.-K. Plattner, M. Tignor, S.K. Allen, J. Boschung, A. Nauels, Y. Xia, V. Bex and P.M. Midgley (eds.)]. Cambridge University Press, Cambridge, United Kingdom and New York, NY, USA, 1535 pp.

4. Carslaw, K. S.; Lee, L. A.; Reddington, C. L.; Pringle, K. J.; Rap, A.; Forster, P. M.; Mann, G. W.; Spracklen, D. V.; Woodhouse, M. T.; Regayre, L. A.; Pierce, J. R., Large contribution of natural aerosols to uncertainty in indirect forcing. *Nature* **2013**, 503 (7474), 67-71.

5. Seinfeld, J. H.; Bretherton, C.; Carslaw, K. S.; Coe, H.; DeMott, P. J.; Dunlea, E. J.; Feingold, G.; Ghan, S.; Guenther, A. B.; Kahn, R. *et al.*, Improving our fundamental understanding of the role of aerosol–cloud interactions in the climate system. *Proc. Natl. Acad. Sci.* **2016**, 113 (21), 5781-5790.

6. Twomey, S., The Influence of Pollution on the Shortwave Albedo of Clouds. *J. Atmos. Sci.* **1977**, 34 (7), 1149-1152.

7. Lohmann, U.; Feichter, J., Global indirect aerosol effects: a review. *Atmos. Chem. Phys*. **2005**, 5 (3), 715-737.

8. Stevens, B.; Feingold, G., Untangling aerosol effects on clouds and precipitation in a buffered system. *Nature* **2009**, 461 (7264), 607-613.

9. Kim, K.-H.; Kabir, E.; Kabir, S., A review on the human health impact of airborne particulate matter. *Environ. Int.* **2015**, 74, 136-143.

10. Sorjamaa, R.; Laaksonen, A., The influence of surfactant properties on critical supersaturations of cloud condensation nuclei. *J. Aerosol Sci.* **2006**, 37 (12), 1730-1736.

11. Clifford, D.; Bartels-Rausch, T.; Donaldson, D. J., Suppression of aqueous surface hydrolysis by monolayers of short chain organic amphiphiles. *Phys. Chem. Chem. Phys.* **2007**, 9 (11), 1362-9.

12. Prisle, N. L.; Raatikainen, T.; Sorjamaa, R.; Svenningsson, B.; Laaksonen, A.; Bilde, M., Surfactant partitioning in cloud droplet activation: a study of C8, C10, C12 and C14 normal fatty acid sodium salts. *Tellus B: Chem. Phys. Meteor.* **2008**, 60 (3), 416-431.

13. Ma, X.; Chakraborty, P.; Henz, B. J.; Zachariah, M. R., Molecular Dynamic Simulation of Dicarboxylic Acid Coated Aqueous Aerosol: Structure and Processing of Water Vapor. *Phys. Chem. Chem. Phys.* **2011**, 13 (20), 9374-9384.

14. Kong, X. R.; Papagiannakopoulos, P.; Thomson, E. S.; Markovic, N.; Pettersson, J. B. C., Water Accommodation and Desorption Kinetics on Ice. *J. Phys. Chem. A* **2014**, 118 (22), 3973-3979.

15. Thomson, E. S.; Kong, X.; Markovic, N.; Papagiannakopoulos, P.; Pettersson, J. B. C., Collision Dynamics and Uptake of Water on Alcohol-Covered Ice. *Atmos. Chem. Phys.* **2013**, 13 (4), 2223-2233.

16. Kong, X.; Toubin, C.; Habartova, A.; Pluharova, E.; Roeselova, M.; Pettersson, J. B. C., Rapid Water Transport through Organic Layers on Ice. *J. Phys. Chem. A* **2018**, 122 (21), 4861-4868.

17. Shiraiwa, M.; Ammann, M.; Koop, T.; Poschl, U., Gas Uptake and Chemical Aging of Semisolid Organic Aerosol Particles. *Proc. Natl. Acad. Sci. U S A* **2011**, 108 (27), 11003-11008.

18. Reid, J. P.; Bertram, A. K.; Topping, D. O.; Laskin, A.; Martin, S. T.; Petters, M. D.; Pope, F. D.; Rovelli, G., The Viscosity of Atmospherically Relevant Organic Particles. *Nat. Commun.* **2018**, 9 (1), 956.

19. Jimenez, J. L.; Canagaratna, M. R.; Donahue, N. M.; Prevot, A. S.; Zhang, Q.; Kroll, J. H.; DeCarlo, P. F.; Allan, J. D.; Coe, H.; Ng, N. L. *et al.*, Evolution of Organic Aerosols in the Atmosphere. *Science* **2009**, 326 (5959), 1525-1529.

20. Ehn, M.; Thornton, J. A.; Kleist, E.; Sipilä, M.; Junninen, H.; Pullinen, I.; Springer, M.; Rubach, F.; Tillmann, R.; Lee, B. *et al.*, A Large Source of Low-Volatility Secondary Organic Aerosol. *Nature* **2014**, 506 (7489), 476-479.

21. Tröstl, J.; Chuang, W. K.; Gordon, H.; Heinritzi, M.; Yan, C.; Molteni, U.; Ahlm, L.; Frege, C.; Bianchi, F.; Wagner, R. *et al.*, The role of low-volatility organic compounds in initial particle growth in the atmosphere. *Nature* **2016**, 533 (7604), 527-531.

22. Guenther, A. B.; Jiang, X.; Heald, C. L.; Sakulyanontvittaya, T.; Duhl, T.; Emmons, L. K.; Wang, X., The Model of Emissions of Gases and Aerosols from Nature version 2.1 (MEGAN2.1): an extended and updated framework for modeling biogenic emissions. *Geosci. Model Dev.* **2012**, 5 (6), 1471-1492.

23. Finlayson-Pitts, B. J.; Pitts, J. N. J., C*hemistry of the Upper and Lower Atmosphere*. Academic Press: New York, USA, **2000**.

24. Grosjean, D.; Grosjean, E.; Williams, E. L., Atmospheric chemistry of unsaturated alcohols. *Environ. Sci. Technol.* **1993**, 27 (12), 2478-2485.

25. Anderson, L. G.; Lanning, J. A.; Barrell, R.; Miyagishima, J.; Jones, R. H.; Wolfe, P., Sources and sinks of formaldehyde and acetaldehyde: An analysis of Denver's ambient concentration data. *Atmos. Environ.* **1996**, 30 (12), 2113-2123.

26. Chebbi, A.; Carlier, P., Carboxylic acids in the troposphere, occurrence, sources, and sinks: A review. *Atmos. Environ.* **1996**, 30 (24), 4233-4249.

27. Hallquist, M.; Wenger, J. C.; Baltensperger, U.; Rudich, Y.; Simpson, D.; Claeys, M.; Dommen, J.; Donahue, N. M.; George, C.; Goldstein, A. H. *et al.*, The Formation, Properties and Impact of Secondary Organic Aerosol: Current and Emerging Issues. *Atmos. Chem. Phys.* **2009**, 9, 5155-5236.

28. Kolb, C. E.; Cox, R. A.; Abbatt, J. P. D.; Ammann, M.; Davis, E. J.; Donaldson, D. J.; Garrett, B. C.; George, C.; Griffiths, P. T.; Hanson, D. R. *et al.*, An overview of current issues in the uptake of atmospheric trace

gases by aerosols and clouds. *Atmos. Chem. Phys.* **2010**, 10 (21), 10561-10605.

29. Smith, J. M.; Saltsburg, H., Atomic-Beam Scattering from Epitaxially Grown Gold Films. *J. Chem. Phys.* **1964**, 40 (12), 3585-3591.

30. Smith, J. N., Molecular beam scattering from solid surfaces: A critical review. *Surf. Sci.* **1973**, 34 (3), 613-637.

31. Stokes, D. J., *Principles and Practice of Variable Pressure/Environmental Scanning Electron Microscopy (VP-esem).* John Wiley & Sons Ltd.: Padstow, **2009**.

32. Fitzek, H.; Schroettner, H.; Wagner, J.; Hofer, F.; Rattenberger, J., High-Quality Imaging in Environmental Scanning Electron Microscopy-Optimizing the Pressure Limiting System and the Secondary Electron Detection of a Commercially Available ESEM. *J. Microsc.* **2016**, 262 (1), 85-91.

33. Koh, A. L.; Lee, S. C.; Sinclair, R., *Controlled Atmosphere Transmission Electron Microscopy Principles and Practice.* Springer: Heidelberg, **2016**.

34. Stöhr, J., *NEXAFS Spectroscopy*. Springer: **1992**.

35. Ogletree, F. D.; Bluhm, H.; Hebenstreit, E. D.; Salmeron, M. B., Photoelectron Spectroscopy under Ambient Pressure and Temperature Conditions. *Nucl. Instrum. Methods Phys. Res., Sect. A* **2009**, 601 (1-2), 151-160.

36. Velasco-Velez, J. J.; Pfeifer, V.; Havecker, M.; Wang, R.; Centeno, A.; Zurutuza, A.; Algara-Siller, G.; Stotz, E.; Skorupska, K.; Teschner, D. *et al.*, Atmospheric Pressure X-ray Photoelectron Spectroscopy Apparatus: Bridging the Pressure Gap. *Rev. Sci. Instrum.* **2016**, 87 (5), 053121.

37. Scoles, G.; Bassi, D.; Buck, U.; Laine, D. C., *Atomic and Molecular Beam Methods.* Oxford University Press,: Oxford, **1988**.

38. Lancaster, D. K.; Johnson, A. M.; Burden, D. K.; Wiens, J. P.; Nathanson, G. M., Inert Gas Scattering from Liquid Hydrocarbon Microjets. *J. Phys. Chem. Lett.* **2013**, 4 (18), 3045-3049.

39. Johansson, S. M.; Kong, X.; Papagiannakopoulos, P.; Thomson, E. S.; Pettersson, J. B., A Novel Gas-Vacuum Interface for Environmental Molecular Beam Studies. *Rev. Sci. Instrum.* **2017**, 88 (3), 035112.

40. Kong, X. R.; Andersson, P. U.; Thomson, E. S.; Pettersson, J. B. C., Ice Formation via Deposition Mode Nucleation on Bare and Alcohol-Covered Graphite Surfaces. *J. Phys. Chem. C* **2012**, 116 (16), 8964-8974.

41. Andersson, P. U.; Nagard, M. B.; Bolton, K.; Svanberg, M.; Pettersson, J. B. C., Dynamics of argon collisions with water ice: Molecular beam experiments and molecular dynamics simulations. *J. Phys. Chem. A* **2000**, 104 (12), 2681-2688.

42. Kong, X.; Andersson, P. U.; Markovic, N.; Pettersson, J. B. C., *Environmental Molecular Beam Studies of Ice Surface Processes. Proceedings of the 12th International Conference on the Physics and Chemistry of Ice*, Hokkaido University Press. **2010**, 79-88.

43. Johansson, S. M.; Lovric, J.; Kong, X.; Thomson, E. S.; Pettersson, J. B. C., An Experimental and Computational Study of Water Interactions with Condensed Nopinone Surfaces under Atmospherically Relevant Conditions. *J. Phys. Chem. A* **2020**.

44. Bird, G. A., *Molecular Gas Dynamics and the Direct Simulation of Gas Flows.* Oxford University Press: Oxford, **1994**.

45. Arumainayagam, C. R.; Madix, R. J., Molecular Beam Studies of Gas-Surface Collision Dynamics. *Prog. Surf. Sci.* **1991**, 38, 1-102.

46. Kontratev, V. N., *Chemical Kinetics of Gas Reactions*. Pergamon Press: London, England, **1964**.

47. Frenkel, D.; Smit, B., *Understanding Molecular Simulation. Second Edition ed.*; Academic Press: San Diego, **2002**.

48. Lee, A.; Goldstein, A. H.; Kroll, J. H.; Ng, N. L.; Varutbangkul, V.; Flagan, R. C.; Seinfeld, J. H., Gas-Phase Products and Secondary Aerosol Yields from the Photooxidation of 16 Different Terpenes. *J. Geophys. Res.* **2006**, 111 (D17).

49. Fisseha, R.; Spahn, H.; Wegener, R.; Hohaus, T.; Brasse, G.; Wissel, H.; Tillmann, R.; Wahner, A.; Koppmann, R.; Kiendler-Scharr, A.,

Stable Carbon Isotope Composition of Secondary Organic Aerosol from β-pinene Oxidation. *J. Geophys. Res.* **2009**, 114 (D2).

50. Hohaus, T.; Gensch, I.; Kimmel, J.; Worsnop, D. R.; Kiendler-Scharr, A., Experimental Determination of the Partitioning Coefficient of beta-pinene Oxidation Products in SOAs. *Phys. Chem. Chem. Phys.* **2015**, 17 (22), 14796-14804.

51. Kavouras, I. G.; Mihalopoulos, N.; Stephanou, E. G., Formation and Gas/Particle Partitioning of Monoterpenes Photo-Oxidation Products over Forests. *Geophys. Res. Lett.* **1999**, 26 (1), 55-58.

52. Holzinger, R.; Lee, A.; Paw, K. T.; Goldstein, U. A. H., Observations of Oxidation Products above a Forest Imply Biogenic Emissions of Very Reactive Compounds. *Atmos. Chem. Phys.* **2005**, 5, 67-75.

53. Cahill, T. M.; Seaman, V. Y.; Charles, J. M.; Holzinger, R.; Goldstein, A. H., Secondary Organic Aerosols Formed from Oxidation of Biogenic Volatile Organic Compounds in the Sierra Nevada Mountains of California. *J. Geophys. Res.* **2006**, 111 (D16).

54. Palin, L.; Brunelli, M.; Wright, J. P.; Pattison, P.; Fitch, A. N., The Low-Temperature Structure of Nopinone. *Z. Kristallogr.* **2008**, 223, 602-604.

55. Schreiber, F., Structure and growth of self-assembling monolayers. *Prog. Surf. Sci.* **2000**, 65 (5), 151-257.

56. Thomson, E. S.; Kong, X. R.; Andersson, P. U.; Markovic, N.; Pettersson, J. B. C., Collision Dynamics and Solvation of Water Molecules in a Liquid Methanol Film. *J. Phys. Chem. Lett.* **2011**, 2 (17), 2174-2178.

57. Papagiannakopoulos, P.; Kong, X. R.; Thomson, E. S.; Markovic, N.; Pettersson, J. B. C., Surface Transformations and Water Uptake on Liquid and Solid Butanol near the Melting Temperature. *J. Phys. Chem. C* **2013**, 117 (13), 6678-6685.

58. Kong, X. R.; Thomson, E. S.; Papagiannakopoulos, P.; Johansson, S. M.; Pettersson, J. B. C., Water Accommodation on Ice and Organic Surfaces: Insights from Environmental Molecular Beam Experiments. *J. Phys. Chem. B* **2014**, 118 (47), 13378-13386.

59. Papagiannakopoulos, P.; Kong, X. R.; Thomson, E. S.; Pettersson, J. B. C., Water Interactions with Acetic Acid Layers on Ice and Graphite. *J. Phys. Chem. B* **2014**, 118 (47), 13333-13340.

60. Johansson, S. M.; Lovric, J.; Kong, X.; Thomson, E. S.; Papagiannakopoulos, P.; Briquez, S.; Toubin, C.; Pettersson, J. B. C., Understanding Water Interactions with Organic Surfaces: Environmental Molecular Beam and Molecular Dynamics Studies of the Water-Butanol System. *Phys. Chem. Chem. Phys.* **2019**, 21 (3), 1141-1151.

61. Kong, X.; Thomson, E.; Markovic, N.; Pettersson, J. B. C., Dynamics and Kinetics of Methanol - Graphite Interactions at Low Surface Coverage. *Chem. Phys. Chem.* **2019**.

62. Barnes, G. T., Permeation Through Monolayers. *Colloids Surf.* **1997**, 126, 149-158.

63. Haynes, W. M., *Physical Constants of Organic Compounds in CRC Handbook of Chemistry and Physics.* CRC Press, Taylor & Francis Group: Boca Raton, FL, **2014.**

64. Andersson, P. U.; Nagard, M. B.; Pettersson, J. B. C., Molecular beam studies of HCl interactions with pure and HCl-covered ice surfaces. *J. Phys. Chem. B* **2000**, 104 (7), 1596-1601.

65. Johansson, S. M.; Kong, X.; Thomson, E. S.; Hallquist, M.; Pettersson, J. B. C., The Dynamics and Kinetics of Water Interactions with a Condensed Nopinone Surface. *J. Phys. Chem. A* **2017**, 121 (35), 6614-6619.

66. Johansson, S. M.; Lovric, J.; Kong, X.; Thomson, E. S.; Pettersson, J. B. C., Water Interactions with Condensed Carboxylic Acids: Adsorption and Desorption of Water on Valeric Acid Surfaces. *Phys. Chem. Chem. Phys.* **2020**.

67. Gilde, A.; Siladke, N.; Lawrence, C. P., Molecular Dynamics Simulations of Water Transport through Butanol Films. *J. Phys. Chem. A* **2009**, 113 (30), 8586-8590.